Effect of Lattice Vibrations in a Multiple-Scattering Description of Low-Energy Electron Diffraction. I. Formal Perturbation Theory*

C. B. DUKE AND G. E. LARAMORE†
Department of Physics, Materials Research Laboratory and Coordinated Science Laboratory, University of Illinois, Urbana-Champaign, Illinois 61801
(Received 19 June 1970)

A diagrammatic version of perturbation theory is developed for the description of the influence of lattice vibrations on the elastic and inelastic scattering cross sections of low-energy electrons from surfaces of single-crystal solids. The formalism describes the effects on the cross sections of a thermodynamic-equilibrium distribution of both bulk and surface phonon modes. The relationships between our general formalism and the conventional single-scattering analysis of inelastic electron-solid scattering are displayed. Multiple-scattering and virtual-phonon emission from a given ion core are included in the theory via vertex renormalizations of the electron–ion-core scattering vertices. Propagator renormalization is estimated to be small and consequently neglected. The diagrammatic contributions to the elastic scattering cross section are summed explicitly using the approximation that diagrams with internal phonon propagators are small relative to those without such propagators. In this approximation we obtain a set of coupled integral equations for appropriately renormalized scattering amplitudes describing elastic electron scattering from planar layers of ion cores.

I. INTRODUCTION

Despite a history of experimental work extending over more than five decades, a reasonably adequate theoretical model of the elastic scattering of low-energy ($E \lesssim 500$ eV) electrons from solid surfaces has been given only in the past few years. The primary reason underlying the lagging development of the theory is the failure of any truly elementary model to incorporate all of the essential features of the scattering process. In contrast with the situations described by the well-developed theories of x-ray and neutron scattering from solids, the interactions between the incident electron and the constituents of the solid are not weak and consequently cannot be described adequately by linear-response theory. Because of the large electron–ion-core scattering cross sections, a description of the multiple scattering between the incident electron and the ion cores of the solid is an essential ingredient of a theory of low-energy electron diffraction (LEED).[1–7] In addition, the interaction of the incident electron with the valence electrons in the solid causes a rapid inelastic collision damping of the elastic wave field within 5–10 Å of the surface.[8] Consequently the effects of both multiple scattering and inelastic collisions must be described in any adequate theory of LEED.[8,9] A phenomenological description of the influence of inelastic collisions on the elastic scattering cross sections has provided,[9] for the first time, an adequate model description of the qualitative features of experimental data. This paper is the first in a series of four in which we refine and extend the inelastic collision model[8,9] to incorporate a microscopic description of inelastic as well as elastic scattering processes into a description of the interaction of low-energy electrons with solid surfaces. In this first paper emphasis is placed on the general features of the formalism (which, e.g., apply to atom and ion-solid interactions as well as LEED). In the second paper we analyze the influence of lattice vibration on elastic LEED with emphasis on the sensitivity of the model predictions to the boundary conditions at the surface. In the third paper we extend the model perturbation-theory analysis to calculate the inelastic scattering differential cross sections associated with large-energy electronic (i.e., $\Delta E \gtrsim 1$ eV) loss processes in the solid. In the final paper we apply the extended theory to describe the two-step inelastic diffraction of electrons from W(100) and Al(100).

Although we utilize standard techniques of quantum field theory in the construction of our model, the nature of electronic interactions at surfaces necessitates that our applications of these techniques differ from the customary "uniform-medium" applications in several significant respects. The combined influence of the aperiodicity of the potential normal to the surface and the inelastic collision damping renders the bulk momentum conservation laws inadequate for electron (atom, ion) surface scattering. Thus, a major aspect of our diagrammatic analysis is the retention of sums over scattering sites until the final stages of the calculation so that appropriate momentum conservation laws are incorporated in the analysis. For convenience in this first version of the inelastic collision model we continue to use plane-wave basis functions for the perturbation theory. The deficiences of such a basis are well known.[8] We expect to eliminate them by use of a distorted-wave basis in the next extension of the model.

The second distinction between our analysis and bulk applications of quantum-field-theory methods centers around the special features of electron diffraction from a vibrating lattice. As the lattice vibrations are low-energy atomistic excitations, $\hbar\omega \lesssim 10$ meV, they must be described by a finite-temperature theory. However, unlike the description of transport processes, the

thermodynamic probability of electron states at the energy of the incident electron ($E-E_F \gtrsim 5$ eV) being occupied is negligible. Therefore we construct a collision theory in which the occupancy of the phonon states is described using the techniques of finite-temperature many-body theory and the occupancy of states of the incident electron is characteristic of a fermion whose energy is high relative to the energies of the occupied electronic states. In particular, the initial and final states of the electron are determined by the experimental apparatus and hence are not subject to thermodynamic averaging.

Having noted the distinctions between our general analysis and previous ones, let us inquire as to which aspects of this analysis we wish to develop for comparison with experimental data. An important aspect of electron-phonon interactions is the smallness of most phonon energies ($\hbar\omega \lesssim 10$ meV) relative to the energy resolution of typical LEED instruments ($\Delta E \gtrsim 0.5$ eV). Therefore it appears most sensible to begin by calculating the temperature dependence of the elastic scattering rather than by examining features of the inelastic scattering cross sections. The temperature dependence of LEED intensity and angular profiles is a well-documented experimental fact.[10–15] The conventional analyses[11–17] of these observations utilize linear-response theory (i.e., the Born approximation), which, as noted above, is demonstrably inadequate[8,9,18] for describing elastic scattering intensity profiles. Thus, a major result of this paper (Sec. VI) is the derivation of a set of integral equations describing multiple elastic scattering of the incident electron from a vibrating lattice in the presence of strong inelastic collision damping due to high-energy (electronic) loss processes. The solution of these equations is presented in the second paper of the series.

The analysis presented in this paper is organized by first defining the model Hamiltonian and specifying the electron-electron–interaction-induced propagator renormalization in Sec. II. The perturbation-theory analysis of the electron–rigid-lattice and electron-phonon interactions described by the model Hamiltonian is developed in Sec. III. This analysis is based on a description of the electron–ion-core interactions using the Dirac (interaction) representation.[19] A general diagrammatic prescription for the elastic and inelastic differential cross sections is developed in a way that permits the inclusion of the effects of surface as well as bulk phonon modes.[20–22] In Sec. IV we show that our prescription yields a convenient form of the usual Born-approximation analysis[11–17] when we neglect multiple-scattering diagrams. In Sec. V we make use of the fact that the incident electron has a velocity much larger than the velocity of an ion core to write a renormalized vertex function for the individual electron–ion-core scattering amplitudes. In Sec. VI we isolate and explicitly sum the dominant diagrams for the elastic scattering cross section. Finally, we summarize our results in Sec. VII.

II. MODEL HAMILTONIAN

We take the Hamiltonian describing the system of incident electron plus solid as

$$\mathcal{H}=\mathcal{H}_0{}^i+\mathcal{H}_0{}^e+\mathcal{H}_1, \tag{1}$$

where $\mathcal{H}_0{}^i$ is the Hamiltonian describing the motion of the ion cores in the solid, $\mathcal{H}_0{}^e$ is the Hamiltonian describing the motion of the incident electron in the absence of any interaction with the ion cores, and $\mathcal{H}_1$ is the perturbative part of the Hamiltonian that describes the interaction between the incident electron and the ion cores.

We treat the motion of the ion cores in the harmonic approximation. Within the framework of this approximation, the Hamiltonian describing the ion core motion is given by

$$\mathcal{H}_0{}^i=\sum_{l_1}-(\hbar^2\nabla_{l_1}{}^2/2M_{l_1})+\tfrac{1}{2}\sum_{l_1,l_2}u_{l_1}{}^\alpha V^{\alpha\beta}(l_1,l_2)u_{l_2}{}^\beta, \tag{2a}$$

$$V^{\alpha\beta}(l_1,l_2)=(\partial/\partial R_{l_1}{}^{0,\alpha})(\partial/\partial R_{l_2}{}^{0,\beta})\times E(\mathbf{R}_{l_1}{}^0,\mathbf{R}_{l_2}{}^0,\ldots,\mathbf{R}_{l_N}{}^0). \tag{2b}$$

The quantity $E(\mathbf{R}_{l_1}{}^0,\mathbf{R}_{l_2}{}^0,\ldots,\mathbf{R}_{l_N}{}^0)$ is the total interaction energy of the system of ions, and α and β are Cartesian indices with the convention of summing over repeated indices being used;

$$\mathbf{R}_l=\mathbf{R}_l{}^0+\mathbf{u}_l \tag{3}$$

is the actual position of the lth ion, which is written in terms of its equilibrium position $\mathbf{R}_l{}^0$ and its displacement from equilibrium $\mathbf{u}_l$.

Far outside the solid we expect the motion of the incident electron to be described by the free-electron Hamiltonian

$$\mathcal{H}_0{}^e=-\hbar^2\nabla^2/2m. \tag{4a}$$

As the incident electron approaches the surface of the solid its interactions with conduction electrons become important (for instance, they are the source of the image force). We ignore this added complexity and consider only the effect of the conduction electrons when the incident electron is inside the metal. The Hamiltonian describing the motion of the electrons inside the metal in the absence of any interaction with the ion cores is taken to be

$$\mathcal{H}_0{}^e=-\frac{\hbar^2\nabla^2}{2m}+\sum_i\frac{e^2}{|\mathbf{r}-\mathbf{r}_i|}-\sum_i\frac{\hbar^2\nabla_i{}^2}{2m}+\sum_{\langle ij\rangle}\frac{e^2}{|\mathbf{r}_i-\mathbf{r}_j|}. \tag{4b}$$

As we are concerned primarily with the effects of phonons, we are not directly interested in the creation of excitations of the conduction electrons (such as plasmons or electron-hole pairs). However, these excitations remove incident electrons from a beam of definite energy. We take this into account by using the propagator renormalization described in Refs. 8 and 9.

This requires the use of a complex self-energy in the propagator[23] describing the motion of the incident electron inside the solid. Specifically, the matrix element of the propagator between plane-wave states $|\mathbf{k}\rangle$ and $|\mathbf{k}'\rangle$ is taken to be

$$\langle\mathbf{k}'|(E-\mathcal{H}_0{}^e+i\eta)^{-1}|\mathbf{k}\rangle = [E-\epsilon_k-\Sigma(\mathbf{k},E)]^{-1}\delta_{k,k'}\equiv G(\mathbf{k},E), \quad (5)$$

where $\mathcal{H}_0{}^e$ is as given in Eq. (4b), η is a positive infinitesimal,

$$\epsilon_k=\hbar^2k^2/2m, \quad (6)$$

and $\Sigma(\mathbf{k},E)$ is the electronic proper self-energy.[8,9]

The interaction Hamiltonian is given by

$$\mathcal{H}_1=\sum_n v(\mathbf{r}-\mathbf{R}_n)=\sum_n\sum_q \exp[i\mathbf{q}\cdot(\mathbf{r}-\mathbf{R}_n)]v_q{}^n, \quad (7)$$

where $v(\mathbf{r}-\mathbf{R}_n)$ is the interaction between the incident electron and the nth ion core and $v_q{}^n$ is its Fourier transform. We maintain the site dependence of the Fourier transform in order to allow for inequivalent sites. A major problem in any LEED analysis is deciding what to use for $v(\mathbf{r}-\mathbf{R}_n)$. In principle, the $v(\mathbf{r}-\mathbf{R}_n)$ are the self-consistent ion-core potentials of the nuclei immersed in a sea of conduction electrons.[24] In view of the fact that the ion cores near the surface dominate the electron-solid scattering, it seems most practical to assume an empirical form for the $v(\mathbf{r}-\mathbf{R}_n)$ rather than attempt to calculate them from a microscopic model. The influence on electron scattering of the lattice vibrations is described using the rigid-ion model to identify $\mathbf{R}_n$ with the instantaneous position of the nth ion core. The position coordinates $\{\mathbf{R}_n\}$ have an implicit time dependence determined by $\mathcal{H}_0{}^i$.

We use $\mathcal{H}_1$ in its second-quantized form[23]

$$\mathcal{H}_1=\sum_n\sum_{k,q}\exp(-i\mathbf{q}\cdot\mathbf{R}_n)v_q{}^n c_{k+q}{}^\dagger c_k. \quad (8)$$

In Eq. (8) $c_k{}^\dagger$ is the operator describing the creation of the LEED electron in the plane-wave state $|\mathbf{k}\rangle$ and c_k is the corresponding annihilation operator.

In Sec. III we calculate the differential scattering cross section that is predicted by these Hamiltonians.

III. DIFFERENTIAL SCATTERING CROSS SECTION: DIAGRAMMATIC EXPANSION

Our calculation starts with the standard definition[19] of the differential scattering cross section for an electron being scattered from an initial momentum state $\mathbf{k}_i$ to a final momentum state $\mathbf{k}_f$ and for the lattice of ion cores going from a state with initial quantum numbers $\{n_i\}$ to a state with final quantum numbers $\{n_f\}$,

$$\left.\frac{d^2}{d\epsilon\,d\Omega}\right|_{k_i\to k_f,\,\{ni\}\to\{nf\}}=\frac{m^2}{(2\pi\hbar)^3}\frac{|\mathbf{k}_f|}{|\mathbf{k}_i|}\dot{P}_{I\to F}, \quad (9)$$

where $\dot{P}_{I\to F}$ is the transition rate between an initial state $|I\rangle$ and a final state $|F\rangle$ which we take as a product of wave functions describing the lattice and the incident electron,

$$|I\rangle=|\{n_i\}\rangle|\mathbf{k}_i\rangle, \quad (10a)$$

$$|F\rangle=|\{n_f\}\rangle|\mathbf{k}_f\rangle. \quad (10b)$$

In Eq. (9) we have normalized the volume of the system to unity.

It is convenient first to calculate the total transition probability $P_{I\to F}$ and then to relate the result to the transition rate $\dot{P}_{I\to F}$. The transition probability is given by

$$P_{I\to F}=|\Gamma_{I\to F}|^2, \quad (11)$$

where $\Gamma_{I\to F}$ is the probability amplitude for transitions between the initial and final states,

$$\Gamma_{I\to F}=\lim_{t\to\infty,\ t_0\to-\infty}\langle F|S(t,t_0)-1|I\rangle \times\exp[-i(E_I-E_F)t_0/\hbar]. \quad (12)$$

In Eq. (12), $S(t,t_0)$ is the scattering matrix which is defined in terms of the interaction Hamiltonian via

$$S(t,t_0)=\left[\exp\left(-(i/\hbar)\int_{t_0}^{t}dt_1\,\mathcal{H}_1{}^I(t_1)\right)\right]_+, \quad (13)$$

where the "+" subscript denotes the time-ordering operation[25] and the superscript "I" on the interaction Hamiltonian means that its time dependence is to be taken in the interaction representation

$$\mathcal{H}_1{}^I(t)=\exp\left((it/\hbar)(\mathcal{H}_0{}^e+\mathcal{H}_0{}^i)\right)\mathcal{H}_1 \times\exp\left(-(it/\hbar)(\mathcal{H}_0{}^e+\mathcal{H}_0{}^i)\right). \quad (14)$$

However, the cross section given in Eq. (9) is not what is measured in a LEED scattering experiment. In such an experiment only the initial and final momentum and energy of the electron are observed—not the initial and final quantum numbers of the lattice. Hence, what is observed is the sum of all the scattering events defined by averaging over the initial states of the lattice and summing over the final lattice states. Note that the only place the lattice states enter in Eq. (9) is in the transition rate $\dot{P}_{I\to F}$. So the experimentally observed scattering cross section is given by

$$\left.\frac{d^2\sigma}{d\epsilon\,d\Omega}\right|_{k_i\to k_f}=\frac{m^2}{(2\pi\hbar)^3}\frac{|\mathbf{k}_f|}{|\mathbf{k}_i|}\langle\dot{P}_{I\to F}\rangle_T. \quad (15)$$

The total transition probability corresponding to $\langle\dot{P}_{I\to F}\rangle_T$ is given by

$$\langle P_{I\to F}\rangle_T=\sum_{\{ni\}}\sum_{\{nf\}}\rho_{\{ni\}}\langle\{n_f\}|\langle\mathbf{k}_f|S(\infty,-\infty)-1|\mathbf{k}_i\rangle \times|\{n_i\}\rangle\langle\{n_i\}|\langle\mathbf{k}_i|S^\dagger(\infty,-\infty)-1 \times|\mathbf{k}_f\rangle|\{n_f\}\rangle\equiv\langle\langle\mathbf{k}_i|S^\dagger(\infty,-\infty)-1|\mathbf{k}_f\rangle \times\langle\mathbf{k}_f|S(\infty,-\infty)-1|\mathbf{k}_i\rangle\rangle_T. \quad (16)$$

In Eq. (16) $\rho\{n_i\}$ is an equilibrium density matrix[25] which depends only on $\mathcal{H}_0{}^i$, the part of the Hamiltonian describing the ion motion. Therefore the average using $\rho\{n_i\}$ is a thermal average. This is the origin of the subscript "T" on the angular brackets. In order to

evaluate Eq. (16) we make use of an expansion of $S(t, t_0)$ in powers of the interaction,

$$S(t, t_0)=1+\left(-\frac{i}{\hbar}\right)\int_{t_0}^{t} dt_1 \mathcal{H}_1^I(t_1)+\left(-\frac{i}{\hbar}\right)^2\int_{t_0}^{t} dt_1 \int_{t_0}^{t_1} dt_2\, \mathcal{H}_1^I(t_1)\mathcal{H}_1^I(t_2)+\cdots. \tag{17}$$

Substituting Eq. (17) into Eq. (16), we obtain

$$\begin{aligned}\langle P_{I\to F}\rangle_T=&\left\langle \langle \mathbf{k}_i|\left(\frac{i}{\hbar}\right)\int_{-\infty}^{\infty} dt_1'\, \mathcal{H}_1^{I\dagger}(t_1')|\,\mathbf{k}_f\rangle\langle \mathbf{k}_f|\left(-\frac{i}{\hbar}\right)\int_{-\infty}^{\infty} dt_1\, \mathcal{H}_1^I(t_1)|\,\mathbf{k}_i\rangle\right\rangle_T\\
&+\left\langle \langle \mathbf{k}_i|\left(\frac{i}{\hbar}\right)\int_{-\infty}^{\infty} dt_1'\, \mathcal{H}_1^{I\dagger}(t_1')|\,\mathbf{k}_f\rangle\langle \mathbf{k}_f|\left(-\frac{i}{\hbar}\right)^2\int_{-\infty}^{\infty} dt_1 \int_{-\infty}^{t_1} dt_2\, \mathcal{H}_1^I(t_1)\mathcal{H}_1^I(t_2)|\,\mathbf{k}_i\rangle\right.\\
&\left.+\langle \mathbf{k}_i|\left(\frac{i}{\hbar}\right)^2\int_{-\infty}^{\infty} dt_1' \int_{t_1'}^{\infty} dt_2'\, \mathcal{H}_1^{I\dagger}(t_1')\mathcal{H}_1^{I\dagger}(t_2')|\,\mathbf{k}_f\rangle\langle \mathbf{k}_f|\left(-\frac{i}{\hbar}\right)\int_{-\infty}^{\infty} dt_1\, \mathcal{H}_1^I(t_1)|\,\mathbf{k}_i\rangle\right\rangle_T+\cdots. \end{aligned}\tag{18}$$

In Eq. (18) we have shown explicitly terms through third order in the interaction Hamiltonian. The first term on the right-hand side of Eq. (18) yields the familiar first Born-approximation expression for the cross section. The inclusion of the higher-order terms constitutes the new features of our analysis.

Equation (18) illustrates one of the unique features of our theory of LEED which distinguish it from the conventional treatments of elementary treatments of elementary-particle field theory on one hand[19] and finite-temperature many-body theory[25] on the other. Conventional field theory[19] describes transitions between states of specified boson occupation number as described, e.g., by Eq. (9). In finite-temperature many-body theory,[25] the occupation of the electronic as well as boson quantum states are described as a thermodynamic average over an equilibrium distribution. However, in a description of inelastic LEED from a vibrating lattice, the initial and final states of the electron are specified precisely (as in conventional field theory) whereas the boson (lattice-vibration) quantum states are averaged over (as in conventional many-body theory). Therefore Eq. (18) specifies a "mixed" representation in which the quantum states of the lattice are averaged over a equilibrium distribution, but the quantum states of the electron are taken as specified by the electron source ($|\,\mathbf{k}_i\rangle$) and detector ($|\,\mathbf{k}_f\rangle$). This mixed representation leads naturally to the use of (multiple) finite-temperature Green's functions for the lattice motion in our final expression for the cross sections. The expressions obtained thereby are not confined to those predicted by treating the electron-lattice interaction in linear-response theory. Rather, they constitute a diagrammatic description of electron-lattice scattering to arbitrary order in either the electron–rigid-lattice or electron-phonon vertex functions. Simple Born-approximation expressions for electron-lattice scattering[25] are valid only to second order in the electron–rigid-lattice vertex (corresponding, e.g., to primary Bragg peaks in the elastic LEED cross sections). The distorted-wave Born-approximation extension of linear-response theory is valid only to second order in the electron-phonon interaction although it formally includes sums of the elastic scattering diagrams from a rigid lattice to infinite order.

In order to illustrate the details of our perturbation theory, let us examine the term third order in the interaction Hamiltonian. It is the simplest one that illustrates the procedure used in obtaining a diagrammatic expression for the cross section. Using the second-quantitized form for the interaction Hamiltonian given in Eq. (8), we obtain the following expression for the third-order term:

$$\begin{aligned}\langle P_{I\to F}\rangle_T{}^{(3)}=&-\frac{i}{\hbar^3}\sum_{l,m,n}\int_{-\infty}^{\infty} dt_1' \int_{-\infty}^{\infty} dt_1 \int_{-\infty}^{t_1} dt_2\\
&\times\sum_{\mathbf{k}_1',\mathbf{q}_1';\mathbf{k}_1,\mathbf{q}_1;\mathbf{k}_2,\mathbf{q}_2}\exp[i\mathbf{q}_1'\cdot\mathbf{R}_l{}^0-i\mathbf{q}_1\cdot R_m{}^0-i\mathbf{q}_2\cdot\mathbf{R}_n{}^0]\\
&\times v_{\mathbf{q}_1'}{}^{*l}v_{\mathbf{q}_1}{}^m v_{\mathbf{q}_2}{}^n\langle \mathbf{k}_i|\,c_{\mathbf{k}_1'}{}^\dagger(t_1')c_{\mathbf{k}_1'+\mathbf{q}_1'}(t_1')|\,\mathbf{k}_f\rangle\\
&\times\langle \mathbf{k}_f|\,c_{\mathbf{k}_1+\mathbf{q}_1}{}^\dagger(t_1)c_{\mathbf{k}_1}(t_1)c_{\mathbf{k}_2+\mathbf{q}_2}{}^\dagger(t_2)c_{\mathbf{k}_2}(t_2)|\,\mathbf{k}_i\rangle\\
&\times\langle\exp[i\mathbf{q}_1'\cdot\mathbf{u}_l(t_1')]\exp[-i\mathbf{q}_1\cdot\mathbf{u}_m(t_1)]\\
&\times\exp[-i\mathbf{q}_2\cdot\mathbf{u}_n(t_2)]\rangle_T+\text{H.c.}\end{aligned}\tag{19}$$

In Eq. (19) the superscript (3) on $\langle P_{I\to F}\rangle_T{}^{(3)}$ indicates the third-order contribution and the H.c. stands for the Hermitian conjugate of the term explicitly shown. Note that the variables describing the election and the lattice have been separated. This separation implies that we have ignored any effect on the incident electron of the conduction electrons. The ion positions have been written as the equilibrium position plus the instantaneous displacement from equilibrium

$$\mathbf{R}_m(t_1)=\mathbf{R}_m{}^0+\mathbf{u}_m(t_1). \tag{20}$$

As noted eariler, the thermal average involves only the lattice displacement operators $\mathbf{u}_n(t)$. For convenience in discussing elastic scattering, the time dependence of the electron operators in the interaction representation has been denoted by $c_k(t)$ and we write the interaction representation of the lattice displacement operators as $\mathbf{u}_l(t)$.

The central feature of our diagrammatic perturbation theory consists of an expansion of thermal averages of

products of $\exp[i\mathbf{q}\cdot\mathbf{u}(t)]$ factors. We proceed in three steps. First, we prove and utilize an appropriate Wick's expansion of these averages. The terms in this expansion are then expressed as functions of the lattice displacement propagators and resummed into an exponential form. Finally, the exponential forms are expanded again, with each term in this final expansion being associated with an appropriate diagram.

Using a harmonic approximation to describe the dynamics of the lattice displacement operators, the first two steps are accomplished as described in Appendix A. The result for the third-order term in Eq. (19) is given by

$$\begin{aligned}\langle\exp[i\mathbf{q}_1'\cdot\mathbf{u}_l(t_1')]\exp[-i\mathbf{q}_1\cdot\mathbf{u}_m(t_1)]\exp[-i\mathbf{q}_2\cdot\mathbf{u}_n(t_2)]\rangle_T&\\ =\exp[-W_l^*(\mathbf{q}_1')]\exp[-W_m(\mathbf{q}_1)]&\\ \times\exp[-W_n(\mathbf{q}_2)]\exp[iq_1{}^{\alpha'}D^{\alpha\beta}(lt_1';mt_1)q_1{}^{\beta}]&\\ \times\exp[iq_1{}^{\alpha'}D^{\alpha\beta}(lt_1';nt_2)q_2{}^{\beta}]&\\ \times\exp[-iq_1{}^{\alpha}D^{\alpha\beta}(mt_1;nt_2)q_2{}^{\beta}],&\quad(21)\end{aligned}$$

where

$$D^{\alpha\beta}(lt_1';mt_1)=-i\langle u_l{}^{\alpha}(t_1')u_m{}^{\beta}(t_1)\rangle_T \quad (22)$$

and

$$\begin{aligned}W_l(\mathbf{q}_1)&=\tfrac{1}{2}iq_1{}^{\alpha}D^{\alpha\beta}(lt_1;lt_1)q_1{}^{\beta}\\&=\tfrac{1}{2}q_1{}^{\alpha}\langle u_l{}^{\alpha}(t_1)u_l{}^{\beta}(t_1)\rangle_T q_1{}^{\beta}\\&=\tfrac{1}{2}q_1{}^{\alpha}\langle u_l{}^{\alpha}(0)u_l{}^{\beta}(0)\rangle_T q_1{}^{\beta}.\end{aligned}\quad(23)$$

The last step in Eq. (22) follows because of the invariance of the correlation function under a translation in time.[25] If the Debye approximation to the phonon spectrum is taken, $W_l(\mathbf{q}_1)$ becomes the familiar Deybe-Waller factor. However, the effects of surface phonons are included in general form of Eq. (23). The D's defined through Eq. (22) are closely related to phonon propagators[25,26] and we will refer to them as such. They have the same form as the usual time-ordered phonon propagator when the first time is greater than the second time.

Substituting Eq. (21) into Eq. (19), we find

$$\begin{aligned}\langle P_{I\to F}\rangle_T{}^{(3)}=&-\frac{i}{\hbar^3}\sum_{l,m,n}\int_{-\infty}^{\infty}dt_1'\int_{-\infty}^{\infty}dt_1\int_{-\infty}^{t_1}dt_2\\&\times\sum_{\mathbf{k}_1',\mathbf{q}_1';\ \mathbf{k}_1,\mathbf{q}_1;\ \mathbf{k}_2,\mathbf{q}_2}\exp[i\mathbf{q}_1'\cdot\mathbf{R}_l{}^0-i\mathbf{q}_1\cdot\mathbf{R}_m{}^0-i\mathbf{q}_2\cdot\mathbf{R}_n{}^0]\\&\times\{\exp[-W_l(\mathbf{q}_1')]v_{\mathbf{q}_1'}{}^l\}^*\{\exp[-W_m(\mathbf{q}_1)]v_{\mathbf{q}_1}{}^m\}\\&\times\{\exp[-W_n(\mathbf{q}_2)]v_{\mathbf{q}_2}{}^n\}\langle\mathbf{k}_i\,|\,c_{\mathbf{k}_1}{}^{\dagger}(t_1')c_{\mathbf{k}_1'+\mathbf{q}_1'}(t_1')\,|\,\mathbf{k}_f\rangle\\&\times\langle\mathbf{k}_f\,|\,c_{\mathbf{k}_1+\mathbf{q}_1}{}^{\dagger}(t_1)c_{\mathbf{k}_1}(t_1)c_{\mathbf{k}_2+\mathbf{q}_2}{}^{\dagger}(t_2)c_{\mathbf{k}_2}(t_2)\,|\,\mathbf{k}_i\rangle\\&\times\exp[iq_1{}^{\alpha'}D^{\alpha\beta}(lt_1';mt_1)q_1{}^{\beta}]\exp[iq_1{}^{\alpha'}D^{\alpha\beta}(lt_1';nt_2)q_2{}^{\beta}]\\&\times\exp[-iq_1{}^{\alpha}D^{\alpha\beta}(mt_1;nt_2)q_2{}^{\beta}]+\text{H.c.}\end{aligned}\quad(24)$$

We see that the interaction potentials $v_{\mathbf{q}}{}^n$ are renormalized by the "Debye-Waller" factors, i.e.,

$$v_{\mathbf{q}}{}^n\longrightarrow\exp[-W_n(\mathbf{q})]v_{\mathbf{q}}{}^n. \quad (25)$$

This is one of two renormalizations which occur for the "individual-site" amplitudes $v_{\mathbf{q}}{}^n$. The second one consists of summing over multiple scattering at a given site. It is discussed in association with Eq. (59). Both renormalizations exert considerable influence on the cross sections. They are discussed in more detail in Sec. V.

We next turn to the expression of Eq. (24) in diagrammatic form. As noted earlier, this expression is constructed by expanding the $\exp[iq^{\alpha}D^{\alpha\beta}(t',t)q^{\beta}]$ factors and performing the time integrations in each term of the expansion. The propagators are written in terms of their Fourier transforms according to

$$D^{\alpha\beta}(lt_1',mt_1)=\int\frac{d\omega}{2\pi}\exp[-i\omega(t_1'-t_1)]D^{\alpha\beta}(l,m,\omega). \quad (26)$$

We also display explicitly the time dependence of the electron operators in the interaction representation and define the amplitude function

$$\begin{aligned}A(\mathbf{k}_1',\mathbf{q}_1';\mathbf{k}_1,\mathbf{q}_1;\mathbf{k}_2,\mathbf{q}_2;l,m,n;t_1',t_1,t_2)\equiv&\exp[i\mathbf{q}_1'\cdot\mathbf{R}_l{}^0-i\mathbf{q}_1\cdot\mathbf{R}_m{}^0-i\mathbf{q}_2\cdot\mathbf{R}_n{}^0]\\&\times\{\exp[-W_l(\mathbf{q}_1')]v_{\mathbf{q}_1'}{}^l\}^*\{\exp[-W_m(\mathbf{q}_1)]v_{\mathbf{q}_1}{}^m\}\{\exp[-W_n(\mathbf{q}_2)v_{\mathbf{q}_2}{}^n\}\langle\mathbf{k}_i\,|\,\exp[i\mathcal{H}_0{}^e t_1'/\hbar]c_{\mathbf{k}_1'}{}^{\dagger}c_{\mathbf{k}_1'+\mathbf{q}_1'}\\&\times\exp[-i\mathcal{H}_0{}^e t_1'/\hbar]\,|\,\mathbf{k}_f\rangle\langle\mathbf{k}_f\,|\,\exp[i\mathcal{H}_0{}^e t_1/\hbar]c_{\mathbf{k}_1+\mathbf{q}_1}{}^{\dagger}c_{\mathbf{k}_1}\exp[-i\mathcal{H}_0{}^e t_1/\hbar]\exp[i\mathcal{H}_0{}^e t_1/\hbar]c_{\mathbf{k}_2+\mathbf{q}_2}{}^{\dagger}c_{\mathbf{k}_2}\exp[-i\mathcal{H}_0{}^e t_2/\hbar]\,|\,\mathbf{k}_i\rangle.\end{aligned}\quad(27)$$

We now perform some of the time integrals involved in Eq. (24).

Let us first consider the leading term which contains no explicit phonon propagators. It is given by

$$\begin{aligned}P_0{}^{(3)}=&-\frac{i}{\hbar^3}\sum_{l,m,n}\int_{-\infty}^{\infty}dt_1'\int_{-\infty}^{\infty}dt_1\int_{-\infty}^{t_1}dt_2\sum_{\mathbf{k}_1',\mathbf{q}_1';\ \mathbf{k}_1,\mathbf{q}_1;\ \mathbf{k}_2,\mathbf{q}_2}A(\mathbf{k}_1',\mathbf{q}_1';\mathbf{k}_1,\mathbf{q}_1,\mathbf{k}_2,\mathbf{q}_2;l,m,n;t_1',t_1,t_2)+\text{H.c.}\\&=\sum_{l,m,n}\sum_{\mathbf{k}_1',\mathbf{q}_1';\ \mathbf{k}_1,\mathbf{q}_1;\ \mathbf{k}_2,\mathbf{q}_2}\exp[i\mathbf{q}_1'\cdot\mathbf{R}_l{}^0-i\mathbf{q}_1\cdot\mathbf{R}_m{}^0-i\mathbf{q}_2\cdot\mathbf{R}_n{}^0]\\&\times\{\exp(-W_l(\mathbf{q}_1')]v_{\mathbf{q}_1'}{}^l\}^*\{\exp[-W_m(\mathbf{q}_1)]v_{\mathbf{q}_1}{}^m\}\{\exp[-W_n(\mathbf{q}_2)]v_{\mathbf{q}_2}{}^n\}[2\pi\delta(E_i-E_f)]^2\langle\mathbf{k}_i\,|\,c_{\mathbf{k}_1'}{}^{\dagger}c_{\mathbf{k}_1'+\mathbf{q}_1'}\,|\,\mathbf{k}_f\rangle\\&\times\langle\mathbf{k}_f\,|\,c_{\mathbf{k}_1+\mathbf{q}_1}{}^{\dagger}c_{\mathbf{k}_1}(E_i-\mathcal{H}_0{}^e+i\eta)^{-1}c_{\mathbf{k}_2+\mathbf{q}_2}{}^{\dagger}c_{\mathbf{k}_2}\,|\,\mathbf{k}_i\rangle+\text{H.c.}\\&=[2\pi\delta(E_i-E_f)]^2\sum_{l,m,n}\sum_{\mathbf{k}_1}\{\exp[-i(\mathbf{k}_f-\mathbf{k}_i)\cdot\mathbf{R}_l{}^0\exp[-W_l(\mathbf{k}_f-\mathbf{k}_i)]v_{\mathbf{k}_f-\mathbf{k}_i}{}^l\}^*\\&\times\{\exp[-i(\mathbf{k}_f-\mathbf{k}_1)\cdot\mathbf{R}_m{}^0]\exp[-W_m(\mathbf{k}_f-\mathbf{k}_1)]v_{\mathbf{k}_f-\mathbf{k}_1}{}^m\}G(\mathbf{k}_1,E_i)\\&\times\{\exp[-i(\mathbf{k}_1-\mathbf{k}_i)\cdot\mathbf{R}_n{}^0]\exp[-W_n(\mathbf{k}_1-\mathbf{k}_i)]v_{\mathbf{k}_1-\mathbf{k}_i}{}^n\}+\text{H.c.}\end{aligned}\quad(28)$$

The definition of the electron propagator given in Eq. (5) has been used in the final expression in Eq. (28). The E_i and E_f are, respectively, the initial and final energies of the incident electron. An important aspect of our analysis is the explicit retention of the sums over l, m, n in Eq. (28). The conventional procedure in either field theory[19] or many-body[23,25] theory is to use these sums to generate momentum conservation δ functions. In the case of specular reflection of the incident electron, these sums lead to δ functions on the component of momentum parallel to the surface but not on the component normal to the surface. The performance of these sums for the case of elastic scattering is discussed in Sec. VI, and for the case of inelastic scattering in the third paper of this series.

Let us next consider the terms involving only a single phonon propagator. There are three such terms which are given below in Eqs. (29)–(31).

$$P_{1a}^{(3)}=-\frac{i}{\hbar^3}\sum_{l,m,n}\int_{-\infty}^{\infty}dt_1'\int_{-\infty}^{\infty}dt_1\int_{-\infty}^{t_1}dt_2 \times\sum_{\mathbf{k}_1',q_1';\ \mathbf{k}_1,q_1;\ \mathbf{k}_2,q_2}A(\mathbf{k}_1',\mathbf{q}_1';\mathbf{k}_1,\mathbf{q}_1;\mathbf{k}_2,\mathbf{q}_2;l,m,n;t_1',t_1,t_2)iq_1'^{\alpha}D^{\alpha\beta}(lt_1';mt_1)q_1^{\beta}+\text{H.c.}$$

$$=\sum_{l,m,n}\sum_{\mathbf{k}_1}\int\frac{d\omega}{2\pi}[2\pi\delta(E_i-E_f-\hbar\omega)]^2\{\exp[-i(\mathbf{k}_f-\mathbf{k}_i)\cdot\mathbf{R}_l^0]\exp[-W_l(\mathbf{k}_f-\mathbf{k}_i)]v_{\mathbf{k}_f-\mathbf{k}_i}{}^l\}^* \times\{\exp[-i(\mathbf{k}_f-\mathbf{k}_1)\cdot\mathbf{R}_m^0]\exp[-W_m(\mathbf{k}_f-\mathbf{k}_1)]v_{\mathbf{k}_f-\mathbf{k}_1}{}^m\}G(\mathbf{k}_1,E_i) \times\{\exp[-i(\mathbf{k}_1-\mathbf{k}_i)\cdot\mathbf{R}_n^0]\exp[-W_n(\mathbf{k}_1-\mathbf{k}_i)]v_{\mathbf{k}_1-\mathbf{k}_i}{}^n\}i(k_f-k_i)^{\alpha}D^{\alpha\beta}(l,m;\omega)(k_f-k_1)^{\beta}+\text{H.c.}, \quad (29)$$

$$P_{1b}^{(3)}=-\frac{i}{\hbar^3}\sum_{l,m,n}\int_{-\infty}^{\infty}dt_1'\int_{-\infty}^{\infty}dt_1\int_{-\infty}^{t_1}dt_2 \times\sum_{\mathbf{k}_1',q_1';\ \mathbf{k}_1,q_1;\ \mathbf{k}_2,q_2}A(\mathbf{k}_1',\mathbf{q}_1';\mathbf{k}_1,\mathbf{q}_1;\mathbf{k}_2,\mathbf{q}_2;l,m,n;t_1',t_1,t_2)iq_1'^{\alpha}D^{\alpha\beta}(lt_1';nt_2)q_2^{\beta}+\text{H.c.}$$

$$=\sum_{l,m,n}\sum_{\mathbf{k}_1}\int\frac{d\omega}{2\pi}[2\pi\delta(E_i-E_f-\hbar\omega)]^2\{\exp[-i(\mathbf{k}_f-\mathbf{k}_i)\cdot\mathbf{R}_l^0]\exp[-W_l(\mathbf{k}_f-\mathbf{k}_i)]v_{\mathbf{k}_f-\mathbf{k}_i}{}^l\}^* \times\{\exp[-i(\mathbf{k}_f-\mathbf{k}_1)\cdot\mathbf{R}_m^0]\exp[-W_m(\mathbf{k}_f-\mathbf{k}_1)]v_{\mathbf{k}_f-\mathbf{k}_1}{}^m\}G(\mathbf{k}_1,E_i-\hbar\omega) \times\{\exp[-i(\mathbf{k}_1-\mathbf{k}_i)\cdot\mathbf{R}_n^0]\exp[-W_n(\mathbf{k}_1-\mathbf{k}_i)]v_{\mathbf{k}_1-\mathbf{k}_i}{}^n\}i(k_f-k_i)^{\alpha}D^{\alpha\beta}(l,n;\omega)(k_1-k_i)^{\beta}+\text{H.c.}, \quad (30)$$

$$P_{1c}^{(3)}=-\frac{i}{\hbar^3}\sum_{l,m,n}\int_{-\infty}^{\infty}dt_1'\int_{-\infty}^{\infty}dt_1\int_{-\infty}^{t_1}dt_2 \times\sum_{\mathbf{k}_1',q_1';\ \mathbf{k}_1,q_1;\ \mathbf{k}_2,q_2}A(\mathbf{k}_1',\mathbf{q}_1';\mathbf{k}_1,\mathbf{q}_1;\mathbf{k}_2,\mathbf{q}_2;l,m,n;t_1',t_1,t_2)(-i)q_1^{\alpha}D^{\alpha\beta}(m,t_1;n,t_2)q_2^{\beta}+\text{H.c.}$$

$$=\sum_{l,m,n}\sum_{\mathbf{k}_1}\int\frac{d\omega}{2\pi}[2\pi\delta(E_i-E_f)]^2\{\exp[-i(\mathbf{k}_f-\mathbf{k}_i)\cdot\mathbf{R}_l^0]\exp[-W_l(\mathbf{k}_f-\mathbf{k}_i)]v_{\mathbf{k}_f-\mathbf{k}_i}{}^l\}^* \times\{\exp[-i(\mathbf{k}_f-\mathbf{k}_1)\cdot\mathbf{R}_m^0]\exp[-W_m(\mathbf{k}_f-\mathbf{k}_1)]v_{\mathbf{k}_f-\mathbf{k}_1}{}^m\}G(\mathbf{k}_1,E_i-\hbar\omega) \times\{\exp[-i(\mathbf{k}_1-\mathbf{k}_i)\cdot\mathbf{R}_n^0]\exp[-W_n(\mathbf{k}_1-\mathbf{k}_i)]v_{\mathbf{k}_1-\mathbf{k}_i}{}^n\}(-i)(k_f-k_1)^{\alpha}D^{\alpha\beta}(m,n;\omega)(k_1-k_i)^{\beta}+\text{H.c.} \quad (31)$$

Each of the contributions to $\langle P_{I\to F}\rangle_T$ given in Eqs. (28)–(31) contains the square of an energy δ function. This is a general feature of each contributions to $\langle P_{I\to F}\rangle_T$ which arises from the final time integral in the terms of the expansion of $S^{\dagger}(\infty,-\infty)$ and $S(\infty,-\infty)$. It allows us to relate[27] a given contribution to $\langle P_{I\to F}\rangle_T$ to the corresponding contribution to the transition rate $\langle\dot{P}_{I\to F}\rangle_T$. The δ function squared in Eq. (28) can be written as

$$[2\pi\delta(E_i-E_f)]^2=\frac{2\pi\delta(E_i-E_f)}{\hbar}\int_{-\infty}^{\infty}dt\exp[-it(E_i-E_f)/\hbar]=\frac{2\pi\delta(E_i-E_f)}{\hbar}\int_{-\infty}^{\infty}dt. \quad (32)$$

The energy conservation δ functions occur because we took the limit $t\to\infty$, $t_0\to-\infty$ in Eq. (17). However, the integral in Eq. (31) is really

$$\int_{t_0}^{t}dt=\Delta\tau, \quad (33)$$

where $\Delta\tau$ is the duration of the interaction between the incident electron and the solid. Therefore to obtain the transition rate $\langle\dot{P}_{I\to F}\rangle_T$, defined by

$$\langle\dot{P}_{I\to F}\rangle_T=\langle P_{I\to F}\rangle_T/\Delta\tau, \quad (34)$$

we simply make the replacement

$$[2\pi\delta(E_i-E_f)]^2\to(2\pi/\hbar)\delta(E_i-E_f). \quad (35)$$

This procedure allows us to directly relate a given contribution to $\langle P_{I\to F}\rangle_T$ to the corresponding contribution

to $\langle \dot{P}_{I\to F}\rangle_T$ and hence to the differential scattering cross section given in Eq. (15).

The four contributions to $\langle \dot{P}_{I\to F}\rangle_T$ obtained from Eqs. (28)–(31) are associated with separate (i.e., distinguishable) diagrams in the diagrammatic representation of the perturbation-theory expansion for the cross section. To obtain all possible terms nth order in the interaction that contribute to the thermally averaged differential scattering cross section, we use the following prescription:

(a) Draw two vertical lines, the one on the left being directed upward and the one on the right being directed downward. On these lines distribute n dots with the only restriction being that at least one dot must be on each line. Label each dot with a lattice-site index. The time variable runs upward on both lines.

(b) Completely interior line segments in this drawing (those connecting two dots) represent electron propagators. The four exterior line segments label the initial and final scattering states of the incident electron. Label the incoming line segments with momentum $\mathbf{k}_i$ and energy E_i, and the outgoing line segments with momentum $\mathbf{k}_f$ and energy E_f.

(c) Label each of the interior line segments by a momentum variable ($\mathbf{k}$) and an energy variable (E).

(d) Connect the dots in all possible ways with wavy lines representing phonon propagators. Label each wavy line with a frequency variable (ω).

(e) Construct all topologically distinct diagrams using the preceding instructions.

(f) With each dot on the left-hand line (the upward-directed line) associate a renormalized interaction vertex and phase factor given by

$$f(l;\mathbf{k}_2,\mathbf{k}_1)=\exp[-i(\mathbf{k}_2-\mathbf{k}_1)\cdot\mathbf{R}_l{}^0]\times\exp[-W_l(\mathbf{k}_2-\mathbf{k}_1)]v_{\mathbf{k}_2-\mathbf{k}_1}{}^l, \quad (36)$$

where l is the ion-site label, $\mathbf{k}_1$ is the momentum incoming to the dot, $\mathbf{k}_2$ is the momentum outgoing from the dot, W_l is defined in Eq. (23), and v^l is defined in Eq. (7). For example, the vertex given in Eq. (36) has the diagrammatic representation shown in Fig. 1(a). With a corresponding dot on the right-hand line (the downward-directed line) associate $f^*(l;\mathbf{k}_2,\mathbf{k}_1)$. The quantity $(\mathbf{k}_2-\mathbf{k}_1)$ denotes the momentum transfer at the vertex.

(g) With a wavy line connecting two dots associate a tensor product between the phonon propagator and the momentum transfer at the two dots at the end of the propagator. If both dots lie on either the left-hand line or the right-hand line such as shown in Fig. 1(b), the tensor product is to be multiplied by $(-i)$ to obtain the factor

$$(-i)(k_3-k_2)^\alpha D^{\alpha\beta}(m,n;\omega)(k_2-k_1)^\beta.$$

$D^{\alpha\beta}(m,n;\omega)$ is defined in Eqs. (22) and (26) and an explicit form is given in Appendix A, Eqs. (A25)–(A27). If one of the dots connected by the wavy phonon line lies on the left-hand electron line and the other lies on the right-hand electron line, the tensor product is to be multiplied by $(+i)$. For example, the wavy line in Fig. 1(c) is associated with the factor

$$i(k_5-k_4)^\alpha D^{\alpha\beta}(l,n;\omega)(k_2-k_1)^\beta.$$

With each set of j wavy lines connecting the same dots associate a factor of $1/j!$. This factor arises from the factorials occurring in the expansion of the exponentials of the phonon propagators which occur in Eq. (24).

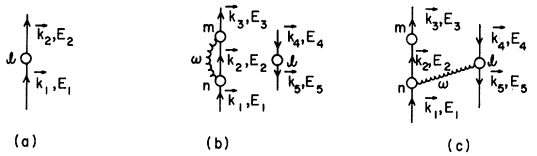

FIG. 1. Diagrams illustrating the rules in the diagrammatic prescription for the differential scattering cross section. (a) represents the vertex given in Eq. (36), (b) illustrates a phonon propagator that does not link the two sides of the diagram, and (c) illustrates a phonon propagator that links the two sides of the diagram. "Bare" vertices $v_q{}^n$ are designated by open dots.

(h) With each interior line segment in the left-hand line we associate a retarded electron propagator, Eq. (5), and with each interior line segment in the right-hand line we associate an advanced electron propagator, Eq. (39). The energy and momentum of the propagator are specified by the labels on the line segment.

(i) With each dot we associate an energy-conserving δ function,

$$2\pi\delta(E_1-E_2-\sum_\alpha \epsilon_\alpha\hbar\omega_\alpha),$$

where E_1 is the energy variable of the incoming electron propagator, E_2 is the energy variable of the outgoing electron propagator, and ω_α is the frequency variable for a phonon line attached to the dot. $\epsilon_\alpha=+1$ for an outgoing phonon line and $\epsilon_\alpha=-1$ for an incoming phonon line. (The terms "incoming" and "outgoing" are defined in the same sense as the direction arrow on the electron propagators. Phonon lines joining the two sides of the diagram are by definition "outgoing" at each vertex.) The sum is over all such phonon lines.

(j) Multiply the factors associated with each diagram by

$$[m^2/(2\pi\hbar)^3]|\mathbf{k}_f|/|\mathbf{k}_i|[2\pi\hbar\delta(E_i-E_f-\sum_\gamma \hbar\omega_\gamma)]^{-1},$$

where the ω_γ are the frequency variables of the phonon propagators connecting the left-hand line to the right-hand line. Sum over all energy and momentum labels for the electron propagators and all frequency variables labeling the phonon propagators.

(k) Finally, sum over all site indices labeling the dots.

To illustrate this prescription let us consider the

FIG. 2. Representative diagrams in the interaction potential expansion for the differential scattering cross section. (a) represents Eq. (36) and (b) represents Eq. (37). (b) is the Hermitian conjugate diagram to (a).

diagram in Fig. 2(a). Its contribution to the differential scattering cross section is given by

$$\left(\frac{d^2\sigma}{d\epsilon\, d\Omega}\right)^{(3)}_{1b} = \sum_{l,m,n}\sum_{\mathbf{k}_1}\int\frac{dE_1}{2\pi}\int\frac{d\omega}{2\pi}$$
$$\times\left(\frac{m^2}{(2\pi\hbar)^3}\frac{|\mathbf{k}_f|}{|\mathbf{k}_i|}[2\pi\hbar\delta(E_i-E_f-\hbar\omega)]^{-1}\right)$$
$$\times[f(n;\mathbf{k}_1,\mathbf{k}_i)2\pi\delta(E_i-E_1-\hbar\omega)]$$
$$\times G(\mathbf{k}_1,E_1)[f(m;\mathbf{k}_f,\mathbf{k}_1)2\pi\delta(E_f-E_1)]$$
$$\times[f^*(l;\mathbf{k}_f,\mathbf{k}_i)2\pi\delta(E_i-E_f-\hbar\omega)](+i)$$
$$\times(\mathbf{k}_f-\mathbf{k}_i)^\alpha D^{\alpha\beta}(l,n;\omega)(k_1-k_i)^\beta$$
$$=\frac{m^2}{(2\pi\hbar^2)^2}\frac{|\mathbf{k}_f|}{|\mathbf{k}_i|}\sum_{l,m,n}\sum_{\mathbf{k}_1}\int\frac{d\omega}{2\pi}\delta(E_i-E_f-\hbar\omega)$$
$$\times f(n;\mathbf{k}_1,\mathbf{k}_i)G(\mathbf{k}_1,E_i-\hbar\omega)f(m;\mathbf{k}_f,\mathbf{k}_1)f^*(l;\mathbf{k}_f,\mathbf{k}_i)$$
$$\times i(k_f-k_i)^\alpha D^{\alpha\beta}(l,n;\omega)(k_1-k_i)^\beta. \quad (37)$$

Equation (37) is simply the contribution to the differential scattering cross section that comes from the term explicitly written on the right-hand side of Eq. (30). The Hermitian conjugate term has the diagrammatic representation shown in Fig. 2(b), which may be explicitly written as

$$\left(\frac{d^2\sigma}{d\epsilon\, d\Omega}\right)^{(3)*}_{1b} = \sum_{l,m,n}\sum_{\mathbf{k}_1}\int\frac{dE_1}{2\pi}\int\frac{d\omega}{2\pi}$$
$$\times\left(\frac{m^2}{(2\pi\hbar)^3}\frac{|\mathbf{k}_f|}{|\mathbf{k}_i|}[2\pi\hbar\delta(E_i-E_f-\hbar\omega)]^{-1}\right)$$
$$\times[f^*(n;\mathbf{k}_1,\mathbf{k}_i)2\pi\delta(E_i-E_1-\hbar\omega)]$$
$$\times G^*(\mathbf{k}_1,E_1)[f^*(m;\mathbf{k}_f,\mathbf{k}_1)2\pi\delta(E_f-E_1)]$$
$$\times[f(l;\mathbf{k}_f,\mathbf{k}_i)2\pi\delta(E_i-E_f-\hbar\omega)]$$
$$\times(+i)(k_f-k_i)^\alpha D^{\alpha\beta}(n,l;\omega)(k_1-k_i)^\beta$$
$$=\frac{m^2}{(2\pi\hbar^2)^2}\frac{|\mathbf{k}_f|}{|\mathbf{k}_i|}\sum_{l,m,n}\sum_{\mathbf{k}_1}\int\frac{d\omega}{2\pi}\delta(E_i-E_f-\hbar\omega)$$
$$\times f^*(n;\mathbf{k}_1,\mathbf{k}_i)G^*(\mathbf{k}_1,E_i-\hbar\omega)f^*(m,\mathbf{k}_f,\mathbf{k}_1)$$
$$\times f(l;\mathbf{k}_f,\mathbf{k}_i)i(k_f-k_i)^\alpha D^{\alpha\beta}(n,l;\omega)(k_1-k_i)^\beta. \quad (38)$$

The retarded electron propagator appearing in Eq. (37) is defined by Eq. (5), whereas the advanced electron propagator in Eq. (38) simply is

$$G^*(\mathbf{k},E)=[E-\epsilon_k-\Sigma^*(\mathbf{k},E)]^{-1}. \quad (39)$$

Note that $iD^{\alpha\beta}(l,n;\omega)$ is real so that Eq. (38) is truly the Hermitian conjugate of Eq. (37). Our use of the "conventional" definition[25,26] of the phonon propagator, Eq. (22), requires us to carry the extra factor of "i" along. As described below Eq. (28), our diagrammatic prescription does not provide the interaction vertices. Analytically, we have built this result into the theory by going over to a diagrammatic formulation prior to performing the lattice sums. This was necessary because of the symmetry-breaking property of the surface. In a "bulk" system we could Fourier transform the phonon propagator in space, perform the lattice sums, and obtain momentum conservation to within a reciprocal-lattice vector. But because of the surface, we can Fourier transform only in the plane parallel to the surface. Consequently, the model predicts conservation only of the component of momentum parallel to the surface to within a reciprocal-lattice vector describing the two-dimension periodicity parallel to the surface. This point will be discussed further in Sec. V. We close this section by giving in Fig. 3 the diagrammatic equation for the thermally averaged differential scattering cross section. The square-box vertices correspond to expressions like Eq. (24) in which the phonon propagators appear in exponents. We have not found it practical to work directly with these exponential expressions and consequently use expansions like those designated in the last two lines of Fig. 3.

IV. DIFFERENTIAL SCATTERING CROSS SECTION: BORN APPROXIMATION

Because of the considerable discussion devoted to it in the literature,[11–17] we consider next the Born approximation to the differential scattering cross section. In the diagrammatic language of Fig. 3, the cross section is represented by the sum of all two point diagrams.

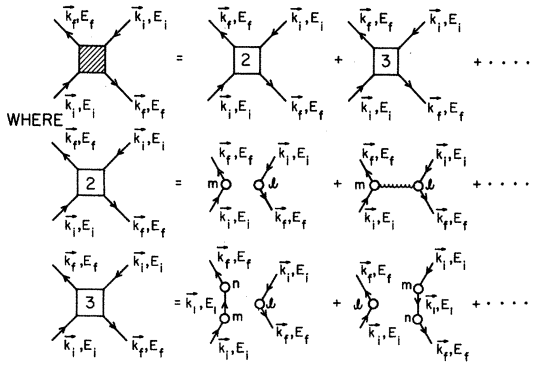

FIG. 3. Diagrammatic equation for the differential scattering cross section in terms of the power to which the renormalized interaction potential is raised.

Taking

$$E_i - E_f = W \tag{40}$$

as the energy lost by the incident electron during the scattering process, we find

$$\left.\frac{d^2\sigma}{d\epsilon\, d\Omega}\right|_{\mathbf{k}_i\to\mathbf{k}_f} = \frac{m^2}{(2\pi\hbar^2)^2}\left[\frac{E_i-W}{E_i}\right]^{1/2} \times \sum_{l,m} \exp[-i(\mathbf{k}_f-\mathbf{k}_i)\cdot(\mathbf{R}_m{}^0-\mathbf{R}_l{}^0)]\exp[-W_m(\mathbf{k}_f-\mathbf{k}_i)]v_{\mathbf{k}_f-\mathbf{k}_i}{}^m \exp[-W_l(\mathbf{k}_f-\mathbf{k}_i)]v_{\mathbf{k}_f-\mathbf{k}_i}{}^{*l}$$

$$\times\left(\delta(W)+i\int\frac{d\omega_1}{2\pi}\delta(W-\hbar\omega_1)(k_f-k_i)^\alpha D^{\alpha\beta}(l,m;\omega_1)(k_f-k_i)^\beta+\frac{(i)^2}{2!}\int\frac{d\omega_1}{2\pi}\frac{d\omega_2}{2\pi}\right.$$

$$\left.\times\delta(W-\hbar\omega_1-\hbar\omega_2)(k_f-k_1)^\alpha D^{\alpha\beta}(l,m;\omega_1)(k_f-k_i)^\beta(k_f-k_i)^\gamma D^{\gamma\delta}(l,m;\omega_2)(k_f-k_i)^\delta+\cdots\right). \tag{41}$$

The first term in Eq. (41) gives the elastic scattering cross section. For the case when all sites are equivalent

$$W_m(\mathbf{k}_f-\mathbf{k}_i) = W_l(\mathbf{k}_f-\mathbf{k}_i) \equiv W(\mathbf{k}_f-\mathbf{k}_i) \tag{42}$$

and the elastic scattering cross section exhibits a temperature dependence proportional to $\exp[-2W(\mathbf{k}_f-\mathbf{k}_i)]$. Often experiments are analyzed[11–15] so as to determine an effective value for $W(\mathbf{k}_f-\mathbf{k}_i)$ and hence a measure of the mean-square ion displacement. Such analyses generally are based upon a Debye model of the phonon spectra in the solid and hence determine an effective Debye temperature.[28] The second term in Eq. (41) gives the contribution due to single-phonon processes. Higher-order terms are not explicitly shown.

Using the integral representation for the energy δ functions in Eq. (41), we obtain

$$\left.\frac{d^2\sigma}{d\epsilon\, d\Omega}\right|^{(2)}_{\mathbf{k}_i\to\mathbf{k}_f} = \frac{m^2}{(2\pi\hbar^2)^2}\left[\frac{E_i-W}{E_i}\right]^{1/2} \times \sum_{l,m} \exp[-i(\mathbf{k}_f-\mathbf{k}_i)\cdot(\mathbf{R}_m{}^0-\mathbf{R}_l{}^0)]\exp[-W_m(\mathbf{k}_f-\mathbf{k}_i)]v_{\mathbf{k}_f-\mathbf{k}_i}{}^m \exp[-W_l(\mathbf{k}_f-\mathbf{k}_i)]v_{\mathbf{k}_f-\mathbf{k}_i}{}^{*l}$$

$$\times\left[\int\frac{dt}{2\pi\hbar}\exp[itW/\hbar]+i\int\frac{d\omega_1}{2\pi}\int\frac{dt}{2\pi\hbar}\exp[it(W-\hbar\omega_1)/\hbar](k_f-k_i)^\alpha D^{\alpha\beta}(l,m;\omega_1)(k_f-k_i)^\beta+\frac{(i)^2}{2!}\int\frac{d\omega_1}{2\pi}\frac{d\omega_2}{2\pi}\int\frac{dt}{2\pi\hbar}\right.$$

$$\left.\times\exp[it(W-\hbar\omega_1-\hbar\omega_2)/\hbar](k_f-k_i)^\alpha D^{\alpha\beta}(l,m;\omega_1)(k_f-k_i)^\beta(k_f-k_i)^\gamma D^{\gamma\delta}(l,m;\omega_2)(k_f-k_i)^\delta+\cdots\right]. \tag{43}$$

Using the definition of the Fourier transform given in Eq. (26), i.e.,

$$D^{\alpha\beta}(l,m;t) = \int\frac{d\omega}{2\pi}\exp(-i\omega t)D^{\alpha\beta}(l,m;\omega), \tag{44}$$

we obtain

$$d^2\sigma/d\epsilon\, d\Omega\,|_{\mathbf{k}_i\to\mathbf{k}_f}{}^{(2)} = [m^2/(2\pi\hbar^2)^2][(E_i-W)/E_i]^{1/2}\sum_{l,m}\exp[-i(\mathbf{k}_f-\mathbf{k}_i)\cdot(\mathbf{R}_m{}^0-\mathbf{R}_l{}^0)]$$

$$\times\exp[-W_m(\mathbf{k}_f-\mathbf{k}_i)]v_{\mathbf{k}_f-\mathbf{k}_i}{}^m\exp[-W_l(\mathbf{k}_f-\mathbf{k}_i)]v_{\mathbf{k}_f-\mathbf{k}_i}{}^*\int(dt/2\pi\hbar)\exp[iWt/\hbar]$$

$$\times\{1+i(k_f-k_i)^\alpha D^{\alpha\beta}(l,m;t)(k_f-k_i)^\beta+[(i)/2!][(k_f-k_i)^\alpha D^{\alpha\beta}(l,m;t)(k_f-k_i)^\beta]^2+\cdots\}$$

$$=[m^2/(2\pi\hbar^2)^2][(E_i-W)/E_i]^{1/2}\sum_{l,m}\exp[-i(\mathbf{k}_f-\mathbf{k}_i)\cdot(\mathbf{R}_m{}^0-\mathbf{R}_l{}^0)]$$

$$\times\exp[-W_m(\mathbf{k}_f-\mathbf{k}_i)]v_{\mathbf{k}_f-\mathbf{k}_i}{}^m\exp[-W_l(\mathbf{k}_f-\mathbf{k}_i)]v_{\mathbf{k}_f-\mathbf{k}_i}{}^{*l}\exp[-i(k_f-k_i)^\alpha D^{\alpha\beta}(l,m;t)(k_f-k_i)^\beta]. \tag{45}$$

Equation (45) gives the cross section accurate to second order in the v's but to all orders in the phonon effects. With the limited instrument resolution of present detectors it rarely is possible to directly measure either the elastic or the inelastic differential cross sections for losses due to phonons. The quantity measured experimentally is the quasi-elastic scattering cross section defined by

$$\left.\frac{d\sigma}{d\Omega}\right|^{(2)}_{\text{qe}} = \int_{-\Delta E/2}^{\Delta/E2} dW \left.\frac{d^2\sigma}{d\epsilon\, d\Omega}\right|^{(2)}_{\mathbf{k}_i\to\mathbf{k}_f}, \tag{46}$$

where ΔE is the experimental energy resolution. Taking $\Delta E \gg \hbar\omega$, where $\hbar\omega$ is a typical phonon energy, we always get a contribution from the energy δ functions in Eq. (41) and so we perform the integral over W trivially. We also

assume $E_i \gg \Delta E$ and hence obtain

$$\frac{d\sigma}{d\Omega}\Big|_{\text{qe}}^{(2)} \cong \frac{m^2}{(2\pi\hbar^2)^2}\sum_{l,m}\exp[-i(\mathbf{k}_f-\mathbf{k}_i)\cdot\mathbf{R}_m{}^0-\mathbf{R}_l{}^0)]\exp[-W_m(\mathbf{k}_f-\mathbf{k}_i)]v_{\mathbf{k}_f-\mathbf{k}_i}{}^m\exp[-W_l(\mathbf{k}_f-\mathbf{k}_i)]v_{\mathbf{k}_f-\mathbf{k}_i}{}^{*l}$$
$$\times\left(1+i\int\frac{d\omega_1}{2\pi}(k_f-k_i)^\alpha D^{\alpha\beta}(l,m;\omega)(k_f-k_i)^\beta+\frac{i^2}{2!}\int\frac{d\omega_1}{2\pi}\frac{d\omega_2}{2\pi}\right.$$
$$\left.\times(k_f-k_i)^\alpha D^{\alpha\beta}(l,m;\omega_1)(k_f-k_i)^\beta(k_f-k_i)^\gamma D^{\gamma\delta}(l,m;\omega_2)(k_f-k_i)^\delta+\cdots\right)$$
$$=\frac{m^2}{(2\pi\hbar^2)^2}\sum_{l,m}\exp[-i(\mathbf{k}_f-\mathbf{k}_i)\cdot(\mathbf{R}_m{}^0-\mathbf{R}_l{}^0)]\exp[-W_m(\mathbf{k}_f-\mathbf{k}_i)]v_{\mathbf{k}_f-\mathbf{k}_i}{}^m$$
$$\times\exp[-W_l(\mathbf{k}_f-\mathbf{k}_i)]v_{\mathbf{k}_f-\mathbf{k}_i}{}^{*l}\exp\left(-(\mathbf{k}_f-\mathbf{k}_i)^\alpha\int\frac{d\omega}{2\pi}D^{\alpha\beta}(l,m;\omega)(k_f-k_i)^\beta\right). \quad (47)$$

By definition

$$\int\frac{d\omega}{2\pi}D^{\alpha\beta}(l,m;\omega)=D(l,m;t=0). \quad (48)$$

Therefore we rewrite Eq. (47) as

$$\frac{d\sigma}{d\Omega}\Big|_{\text{qe}}^{(2)}=\frac{m^2}{(2\pi\hbar^2)^2}\sum_{l,m}\exp[-i(\mathbf{k}_f-\mathbf{k}_i)\cdot(\mathbf{R}_m{}^0-\mathbf{R}_l{}^0)]$$
$$\times\exp[-W_m(\mathbf{k}_f-\mathbf{k}_i)]v_{\mathbf{k}_f-\mathbf{k}_i}{}^m$$
$$\times\exp[-W_l(\mathbf{k}_f-\mathbf{k}_i)]v_{\mathbf{k}_f-\mathbf{k}_i}{}^{*l}$$
$$\times\exp[i(k_f-k_i)^\alpha D^{\alpha\beta}(l,m;t=0)(k_f-k_i)^\beta]. \quad (49)$$

Equation (49) is our final expression for the quasi-elastic scattering cross section (in the Born approximation). It constitutes a simple, compact form which describes the temperature dependence of the elastic scattering,[11,13,15] the thermal diffuse scattering,[12] and "multiphonon" scattering.[14] We now turn to a brief outline of its application to the derivation of sum rules for the quasi-elastic scattering cross section which have been proposed by Webb and collaborators[12,14] as approximate relations.

In the Debye model of the solid (see Appendix A)

$$D^{\alpha\beta}(l,m;t)\propto\delta^{\alpha\beta}. \quad (50)$$

Consequently, both $W_l(\mathbf{k}_f-\mathbf{k}_i)$ and

$$F_{l,m}(\mathbf{k}_f-\mathbf{k}_i)\equiv i(k_f-k_i)^\alpha D^{\alpha\beta}(l,n;t=0)(k_f-k_i)^\beta \quad (51)$$

depend only on $|\mathbf{k}_f-\mathbf{k}_i|$. If, in addition, the potentials only depend on the magnitude of the momentum transferred, we can integrate Eq. (49) to determine the total scattering cross section

$$\sigma|_{\text{qe}}{}^{(2)}=\frac{m^2}{(2\pi\hbar^2)^2}\sum_{l,m}\exp[-W_m(|\mathbf{k}_f-\mathbf{k}_i|)]v_{|\mathbf{k}_f-\mathbf{k}_i|}{}^m$$
$$\times\exp[-W_l(|\mathbf{k}_f-\mathbf{k}_i|)]v_{|\mathbf{k}_f-\mathbf{k}_i|}{}^{*l}\exp[F_{lm}(|\mathbf{k}_f-\mathbf{k}_i|)]$$
$$\times\left(\frac{4\pi\sin(|\mathbf{k}_f-\mathbf{k}_i||\mathbf{R}_m{}^0-\mathbf{R}_l{}^0|)}{|\mathbf{k}_f-\mathbf{k}_i||\mathbf{R}_m{}^0-\mathbf{R}_l{}^0|}\right). \quad (52)$$

For any reasonable lattice parameter a and momentum transfer $|\mathbf{k}_f-\mathbf{k}_i|$

$$G_{l,m}(|\mathbf{k}_f-\mathbf{k}_i|)\equiv\frac{4\pi\sin(|\mathbf{k}_f-\mathbf{k}_i||\mathbf{R}_m{}^0-\mathbf{R}_l{}^0|)}{|\mathbf{k}_f-\mathbf{k}_i||\mathbf{R}_m{}^0-\mathbf{R}_l{}^0|} \quad (53)$$

is a very sharply peaked function of $|\mathbf{R}_m{}^0-\mathbf{R}_l{}^0|$. In the limit that $|\mathbf{k}_f-\mathbf{k}_i|a\gg1$, $G_{l,m}$ may be taken as

$$G_{l,m}(|\mathbf{k}_f-\mathbf{k}_i|)\propto\delta_{l,m}, \quad (54)$$

and hence

$$\sigma|_{\text{qe}}{}^{(2)}\propto\sum_m\exp[-2W_m(|\mathbf{k}_f-\mathbf{k}_i|)]$$
$$\times|v_{|\mathbf{k}_f-\mathbf{k}_i|}{}^m|^2\exp[F_{mm}(|\mathbf{k}_f-\mathbf{k}_i|)]=\sum_m|v_{|\mathbf{k}_f-\mathbf{k}_i|}{}^m|^2. \quad (55)$$

The last step follows from Eqs. (23) and (51). Therefore in the limit that (54) is valid, the total cross section for a fixed magnitude $q=|\mathbf{k}_f-\mathbf{k}_i|$ of momentum transfer is independent of the temperature; i.e., all of the strength which is lost from the elastic peak simply is transferred to the phonon sidebands. Perhaps a more familiar form of Eq. (55) is one in which the second exponential is expanded:

$$\sigma|_{\text{qe}}{}^{(2)}\propto\sum_m\exp[-2W_m(|\mathbf{k}_f-\mathbf{k}_i|)]|v_{|\mathbf{k}_f-\mathbf{k}_i|}{}^m|^2$$
$$\times\sum_j[2W_m(|\mathbf{k}_f-\mathbf{k}_i|)]^j/j!. \quad (56)$$

In Eq. (56) the term in $[2W_m(|\mathbf{k}_f-\mathbf{k}_i|)]^j/j!$ is associated with the j phonon process. The sum rule in the form of Eq. (56) was proposed in Refs. 12 and 14 from other considerations and was used there to discuss the thermal diffuse and multiphonon scattering of electrons. The discussion presented in this section relates explicitly the analysis presented in these references to our general theory.

V. DIFFERENTIAL SCATTERING CROSS SECTION: QUASISTATIC APPROXIMATION

In Sec. III we developed a formal diagrammatic theory for the differential scattering cross section which was expressed in terms of the interaction potential

between the incident electron and the ion cores in a single-crystal solid. In order to relate our analysis to that of previous multiple-scattering theories, it is necessary to renormalize the individual electron–ion-core scattering vertices, that is, to rewrite the diagrams in terms of the effective scattering amplitudes for the ion cores. In the earlier rigid-lattice models[1–7] the prescription for this renormalization was obvious. One solves the Schrödinger equation for the scattering from a single ion core and then writes the multiple-scattering formulas in terms of the resulting "energy-shell" scattering amplitudes. However, it is well known[23,25] that this prescription fails in the case of a dynamic rather than static scatterer because off-energy-shell amplitudes are required to completely specify the scattering. In our discussion of electron-phonon interactions we resolve this difficulty by noting that our use of the rigid-ion model in Eq. (7) implies the validity of the adiabatic hypothesis for electronic motion relative to that of the vibrating ion cores. Thus, in constructing our model we already have assumed that electronic relaxation times τ_{el} are much more rapid than the lattice vibration frequencies ω^{-1}. Consequently, we argue that in our model the appropriate vertex renormalization for electronic scattering from a given site is given by first calculating the energy-shell scattering amplitude for a static ion core at that site and subsequently assigning relative phases for electronic scattering from various sites according to the instantaneous locations of the ion cores. A physically sensible plausibility argument for this prescription may be constructed by noting that the velocity of the incident electron is much greater than the thermal velocities of the ion cores. Therefore during a multiple-scattering process involving the electron and a single ion core, the electron "sees" only a stationary ion core, hence the origin of the appellation "quasistatic" approximation. This result would not be true when considering the scattering of a slowly moving particle such as a neutral atom. Presumably one would have to work directly with the general perturbation theory in such a case.

In performing this multiple-scattering renormalization it is necessary to write the expression for the total transition amplitude given by Eq. (12) taking into account the multiple scattering from a single site before performing the thermal average in the expression for the scattering cross section. Ignoring the (irrelevant) phase factor in Eq. (12), we can write

$$\begin{aligned}\Gamma_{I\to F}&=\langle F\mid S(\infty,-\infty)-1\mid I\rangle\\&=\langle F\mid\sum_m\Big[\Big(-\frac{i}{\hbar}\Big)\int_{-\infty}^{\infty}dt_1\sum_{\mathbf{k}_1,\mathbf{q}_1}\exp\{-i\mathbf{q}_1\cdot[\mathbf{R}_m{}^0+\mathbf{u}_m(t_1)]\}v_{\mathbf{q}_1}{}^m c_{\mathbf{k}_1+\mathbf{q}_1}{}^\dagger(t_1)c_{\mathbf{k}_1}(t_1)\\&\quad+\Big(-\frac{i}{\hbar}\Big)^2\int_{-\infty}^{\infty}dt_1\int_{-\infty}^{t_1}dt_2\sum_{\mathbf{k}_1,\mathbf{q}_1;\,\mathbf{k}_2,\mathbf{q}_2}\exp\{-i\mathbf{q}_1\cdot[\mathbf{R}_m{}^0+\mathbf{u}_m(t_1)]-i\mathbf{q}_2\cdot[\mathbf{R}_m{}^0+\mathbf{u}_m(t_2)]\}v_{\mathbf{q}_1}{}^m v_{\mathbf{q}_2}{}^m\\&\qquad\times c_{\mathbf{k}_1+\mathbf{q}_1}{}^\dagger(t_1)c_{\mathbf{k}_1}(t_1)c_{\mathbf{k}_2+\mathbf{q}_2}{}^\dagger(t_2)c_{\mathbf{k}_2}(t_2)+\cdots\Big]\mid I\rangle\\&\quad+\langle F\mid\sum_{m,n;\ m\neq n}\Big(-\frac{i}{\hbar}\Big)^2\int_{-\infty}^{\infty}dt_1\int_{-\infty}^{t_1}dt_2\sum_{\mathbf{k}_1,\mathbf{q}_1;\,\mathbf{k}_2,\mathbf{q}_2}\exp\{-i\mathbf{q}_1\cdot[\mathbf{R}_m{}^0+\mathbf{u}_m(t_1)]-i\mathbf{q}_2\cdot[\mathbf{R}_n{}^0+\mathbf{u}_n(t_2)]\}\\&\qquad\times v_{\mathbf{q}_1}{}^m v_{\mathbf{q}_2}{}^n c_{\mathbf{k}_1+\mathbf{q}_1}{}^\dagger(t_1)c_{\mathbf{k}_1}(t_1)c_{\mathbf{k}_2+\mathbf{q}_2}{}^\dagger(t_2)c_{\mathbf{k}_2}(t_2)\mid I\rangle+\cdots.\end{aligned}\tag{57}$$

In Eq. (57) we have rearranged the perturbation series to group together terms corresponding to successive "scattering" from a single site. In making the "quasistatic" approximation we ignore any motion of the ion during the multiple scattering from a given site. This is equivalent to equating all of the times associated with the ion displacement operators in the single-site multiple-scattering series. We find

$$\begin{aligned}\Gamma_{I\to F}\mid_{qs}&=\langle F\mid\sum_m\Big[\Big(-\frac{i}{\hbar}\Big)\int_{-\infty}^{\infty}dt_1\sum_{\mathbf{k}_1,\mathbf{q}_1}\exp\{-i\mathbf{q}_1\cdot[\mathbf{R}_m{}^0+\mathbf{u}_m(t_1)]\}v_{\mathbf{q}_1}{}^m c_{\mathbf{k}_1+\mathbf{q}_1}{}^\dagger(t_1)c_{\mathbf{k}_1}(t_1)+\Big(-\frac{i}{\hbar}\Big)^2\int_{-\infty}^{\infty}dt_1\int_{-\infty}^{t_2}dt_2\\&\quad\times\sum_{\mathbf{k}_1,\mathbf{q}_1;\,\mathbf{k}_2,\mathbf{q}_2}\exp\{-i(\mathbf{q}_1+\mathbf{q}_2)[\mathbf{R}_m{}^0+\mathbf{u}_m(t_1)]\}v_{\mathbf{q}_1}{}^m v_{\mathbf{q}_2}{}^m c_{\mathbf{k}_1+\mathbf{q}_1}{}^\dagger(t_1)c_{\mathbf{k}_1}(t_1)c_{\mathbf{k}_2+\mathbf{q}_2}{}^\dagger(t_2)c_{\mathbf{k}_2}(t_2)+\cdots\Big]\mid I\rangle\\&\quad+\langle F\mid\sum_{m,n;\ m\neq n}\Big(-\frac{i}{\hbar}\Big)^2\int_{-\infty}^{\infty}dt_1\int_{-\infty}^{t_2}dt_2\sum_{\mathbf{k}_1,\mathbf{q}_1;\,\mathbf{k}_2,\mathbf{q}_2}\exp\{-i\mathbf{q}_1\cdot[\mathbf{R}_m{}^0+\mathbf{u}_m(t_1)]-i\mathbf{q}_2\cdot[\mathbf{R}_n{}^0+\mathbf{u}_n(t_2)]\}\\&\qquad\times v_{\mathbf{q}_1}{}^m v_{\mathbf{q}_2}{}^n c_{\mathbf{k}_1+\mathbf{q}_1}{}^\dagger(t_1)c_{\mathbf{k}_1}(t_1)c_{\mathbf{k}_2+\mathbf{q}_2}{}^\dagger(t_2)c_{\mathbf{k}_2}(t_2)\mid I\rangle+\cdots.\end{aligned}\tag{58}$$

Substituting Eq. (58) into Eq. (16), we find that the analysis is carried out exactly as before except that instead of being identified with the potential $v_{\mathbf{k}_2-\mathbf{k}_1}{}^m$ the interaction vertices now are identified with the energy-shell scattering amplitude for the site. This amplitude is defined to be $t^m(\mathbf{k}_2, \mathbf{k}_1, E_1)$, which satisfies the equation

$$t^m(\mathbf{k}_2, \mathbf{k}_1; E_1) = v_{\mathbf{k}_2-\mathbf{k}_1}{}^m + \sum_{\mathbf{k}} v_{\mathbf{k}_2-\mathbf{k}}{}^m G(\mathbf{k}, E) v_{\mathbf{k}-\mathbf{k}_1}{}^m + \cdots$$
$$= v_{\mathbf{k}_2-\mathbf{k}_1}{}^m + \sum_{\mathbf{k}} v_{\mathbf{k}_2-\mathbf{k}}{}^m G(\mathbf{k}, E_1) t^m(\mathbf{k}, \mathbf{k}_1; E_1). \quad (59)$$

Concomitantly we require that two successive interaction vertices on a given side of a perturbation-theory diagram cannot correspond to the same site since this process is included in the over-all multiple-scattering site renormalization.

In summary, the site-renormalized diagrams are constructed in the way given by the prescription in Sec. IV with the following modifications:

(i) Rule (f) is modified to read as follows: With each dot on the left-hand line (the upward-directed line) associate a site-renormalized interaction vertex and phase factor given by

$$B(l; \mathbf{k}_2, \mathbf{k}_1; E_1) = \exp[-i(\mathbf{k}_2-\mathbf{k}_1)\cdot R_l{}^0]$$
$$\times \exp[-W_l(\mathbf{k}_2-\mathbf{k}_1)] t^l(\mathbf{k}_2, \mathbf{k}_1; E_1), \quad (60)$$

where l is the ion site label, $\mathbf{k}_1$ is the momentum incoming to the dot, and $\mathbf{k}_2$ is the momentum outgoing from the dot. For example, the vertex given in Eq. (60) has the diagrammatic representation shown in Fig. 4(a). With a corresponding dot on the right-hand line (the downward-directed line) associate $B^*(l; \mathbf{k}_2, \mathbf{k}_1; E_1)$. The quantity $(\mathbf{k}_2-\mathbf{k}_1)$ denotes the momentum transfer at the vertex.

(ii) Rule (k) is modified to read as follows: Finally, sum over all site indices, labeling the dots but noting in the summing procedure that two successive dots on the same side of the diagram cannot correspond to the same lattice site.

For illustrative purposes let us consider the diagram in Fig. 4(b). Its contribution to the scattering cross section is

$$\left(\frac{d\sigma}{d\epsilon\, d\Omega}\right)_{1b}^{(3)} = \sum_{l,m,n;\ m\neq n} \sum_{\mathbf{k}_1} \int \frac{dE_1}{2\pi} \int \frac{d\omega}{2\pi} \left(\frac{m^2}{(2\pi\hbar)^3} \frac{|\mathbf{k}_f|}{|\mathbf{k}_i|} [2\pi\hbar\delta(E_i-E_f-\hbar\omega)]^{-1}\right)$$
$$\times [B(n; \mathbf{k}_1, \mathbf{k}_i; E_i) 2\pi\delta(E_i-E_1-\hbar\omega)] G(\mathbf{k}_1, E_1) [B(m; \mathbf{k}_f, \mathbf{k}_1; E_1) 2\pi\delta(E_f-E_1)]$$
$$\times [B^*(l; \mathbf{k}_f, \mathbf{k}_i; E_i) 2\pi\delta(E_i-E_f-\hbar\omega)] (+i)(k_f-k_i)^\alpha D^{\alpha\beta}(l, n; \omega)(k_1-k_i)^\beta$$
$$= [m^2/(2\pi\hbar^2)^2](|\mathbf{k}_f|/|\mathbf{k}_i|) \sum_{l,m,n;\ m\neq n} \sum_{\mathbf{k}_1} \int (d\omega/2\pi)\delta(E_i-E_f-\hbar\omega)$$
$$\times B(n; \mathbf{k}_1, \mathbf{k}_i; E_i) G(\mathbf{k}_1, E_i-\hbar\omega) B(m; \mathbf{k}_f, \mathbf{k}_1; E_i-\hbar\omega) B^*(l; \mathbf{k}_f, \mathbf{k}_i; E_i) (+i)(k_f-k_i)^\alpha D^{\alpha\beta}(l, n; \omega)(k_1-k_i)^\beta. \quad (61)$$

This is simply the site-renormalized version of the diagram in Fig. 2(a).

We next use this site-renormalized perturbation theory to calculate the elastic scattering cross section.

VI. ELASTIC SCATTERING CROSS SECTION

From step (j) of the diagrammatic prescription specified in Sec. III we see that the inelastic scattering cross section associated with an energy loss W is given by the sum of all diagrams with left- and right-hand electron lines linked with an arbitrary number n of phonon propagator lines such that

$$W = \sum_{\gamma=1}^{n} \hbar\omega_\gamma.$$

The elastic scattering cross section is given by the sum of all diagrams such that the left- and right-hand electron lines are unlinked by phonon propagator lines. However, an arbitrary number of phonon propagators linking points on each electron line with other points on the same line can occur in the elastic scattering diagrams. Therefore, in our theory, even the elastic scattering diagrams contain terms of arbitrary order in the electron-phonon coupling constant. An obvious way to systematize this aspect of the theory is to extend our use of the concept of skeletal diagrams to include the influence of electron-phonon interactions as well as electron-electron interactions on the renormalization of

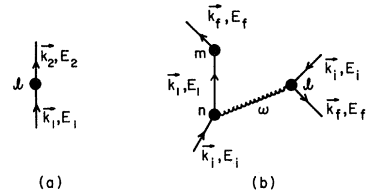

FIG. 4. Site-renormalized diagrams using the quasistatic approximation. (a) illustrates the site-renormalized scattering vertex given in Eq. (51) and (b) is the diagrammatic version of the contribution to the differential scattering cross section given in Eq. (52). Site-renormalized vertices are designated by solid dots.

electronic propagators and "internal" inelastic vertices within a given electron line. Upon investigation, however, the effects associated with these additional renormalizations seem to be small. Therefore we present in Appendix B an order-of-magnitude estimate of the lowest-order diagram containing internal phonon propagators, argue that these effects are sufficiently small to be negligible under most conditions, and turn to developing summation methods for evaluating the combined effect of all multiple-scattering diagrams which contain no internal phonon lines. As the further renormalizations do not lead to results which are useful in the present context, we do not present them here.

We anticipate that the summation of elastic multiple-scattering diagrams can be reduced to the solution of a set of coupled algebraic equations for appropriately defined elastic scattering amplitudes. Beeby already has performed such an analysis for muffin-tin potentials with spherically symmetric ion cores.[7] Our analysis constitutes a generalization of his to arbitrary electron–ion-cores potentials (which, in general, overlap and are nonspherical). In the second paper of this series we show that for such potentials a set of algebraic equations, analogous to Beeby's but in the momentum representation, are the final result of the theory. In this section our final result will be a set of coupled integral equations for various elastic scattering amplitudes.

The approximate diagrammatic equation for the elastic electron-solid differential cross section is indicated in Fig. 5. Denoting the scattering amplitude associated with the shaded "renormalized" vertex by $R(\mathbf{k}_f, \mathbf{k}_i, E_1)$, we write

$$\frac{d^2\sigma}{d\epsilon\, d\Omega}\bigg|^{(0)}_{\mathbf{k}_i\to\mathbf{k}_f} = \frac{m^2}{(2\pi\hbar^2)^2}\delta(E_f-E_i)|\,R(\mathbf{k}_f, \mathbf{k}_i; E_i)|^2. \quad (62)$$

If we denote the single-scattering vertex by $B(n, \mathbf{k}', \mathbf{k}, E_i)$, then $R(\mathbf{k}_f, \mathbf{k}_i, E_1)$ can be written as

$$\begin{aligned}R(\mathbf{k}_f, \mathbf{k}_i; E_i) &= \sum_n B(n; \mathbf{k}_f, \mathbf{k}_i; E_i)\\ &\times \sum_{n,m;\ n\neq m}\ \sum_{\mathbf{k}_1} B(n; \mathbf{k}_1, \mathbf{k}_i; E_i)G(\mathbf{k}_1, E_i)B(m; \mathbf{k}_f, \mathbf{k}_1; E_i)\\ &\times \sum_{n,m,l;\ n\neq m;\ m\neq l}\ \sum_{\mathbf{k}_1,\mathbf{k}_2} B(n; \mathbf{k}_1, \mathbf{k}_i; E_i)G(\mathbf{k}_1, E_i)\\ &\times B(m; \mathbf{k}_2, \mathbf{k}_1, E_i)G(\mathbf{k}_2, E_i)B(l; \mathbf{k}_f, \mathbf{k}_2; E_i)+\cdots. \quad (63)\end{aligned}$$

For notational convenience let us write the interaction vertex as

$$B(n; \mathbf{k}_2, \mathbf{k}_1; E_i) = \exp[-i(\mathbf{k}_2-\mathbf{k}_1)\cdot\mathbf{R}_n{}^0]b_n(\mathbf{k}_2, \mathbf{k}_1; E_i), \quad (64)$$

where

$$b_n(\mathbf{k}_2, \mathbf{k}_1, E_i) = \exp[-W_n(\mathbf{k}_2-\mathbf{k}_1)]t^n(\mathbf{k}_2, \mathbf{k}_1, E_i). \quad (65)$$

We next evaluate the right-hand side of Eq. (63) under the assumption that all scattering sites in a given subplane[7] parallel to the surface are equivalent. That is, we take the potential at a given site to depend only on the distance of that site from the surface. Hence, we label a site both by the subplane in which it lies and by its position within the subplane; i.e., we take

$$n=(\lambda, l), \qquad m=(\lambda_1, l_1), \qquad \text{etc.}, \quad (66)$$

where λ denotes the subplane and l the site position within the subplane. The equilibrium site position becomes

$$\mathbf{R}_n{}^0 = \boldsymbol{\varrho}_l+\lambda\mathbf{a}+d_\lambda\hat{z}, \quad (67)$$

where $\lambda\mathbf{a}$ is the position of the origin in the λth subplane (this is to allow for a shift between successive subplanes),[8,9] $\boldsymbol{\varrho}_l$ is the position of the site relative to the origin, and d_λ is the distance of the λth subplane below the surface which is taken to be the plane $z=0$.

Grouping all sites lying in a given subplane together, we obtain

$$\begin{aligned}&R(\mathbf{k}_f, \mathbf{k}_i; E_i)\\ &= \sum_\lambda \exp[-i(k_{f\perp}-k_{i\perp})d_\lambda - i(\mathbf{k}_{f||}-\mathbf{k}_{i||})\cdot\mathbf{a}_\lambda]\\ &\times\{\sum_l \exp[-i(\mathbf{k}_{f||}-\mathbf{k}_{i||})\cdot\boldsymbol{\varrho}_l]b_\lambda(\mathbf{k}_f, \mathbf{k}_i; E_i)\\ &\sum_{l,l_1;\ l\neq l_1}\ \sum_{\mathbf{k}_1} \exp[-i(\mathbf{k}_{1||}-\mathbf{k}_{i||})\cdot\boldsymbol{\varrho}_l]b_\lambda(\mathbf{k}_1, \mathbf{k}_i; E_i)\\ &\times G(\mathbf{k}_1; E_i)\exp[-i(\mathbf{k}_{f||}-\mathbf{k}_{1||})\cdot\boldsymbol{\varrho}_{l_1}]b_\lambda(\mathbf{k}_f, \mathbf{k}_1; E_i)+\cdots\}\\ &+ \sum_{\lambda,\lambda_1;\ \lambda\neq\lambda_1}\ \sum_{l,l_1} \exp[-i(\mathbf{k}_{1||}-\mathbf{k}_{i||})\cdot(\boldsymbol{\varrho}_l+\mathbf{a}_\lambda)\\ &\quad -i(k_{1\perp}-k_{i\perp})d_\lambda]b_\lambda(\mathbf{k}_1, \mathbf{k}_i; E_i)G(\mathbf{k}_1, E_i)\\ &\times\exp[-i(\mathbf{k}_{f||}-\mathbf{k}_{1||})\cdot(\boldsymbol{\varrho}_l+\mathbf{a}_{\lambda_1})-i(k_{f\perp}-k_{1\perp})d_{\lambda_1}]\\ &\qquad\times b_{\lambda_1}(\mathbf{k}_f, \mathbf{k}_1; E_i)+\cdots. \quad (68)\end{aligned}$$

In Eq. (68) we next perform the sum over the "l" indices. We define the subplane normalization $N_{||}$ by

$$\sum_l \exp[-i(\mathbf{k}_{2||}-\mathbf{k}_{1||})\cdot\boldsymbol{\varrho}_l] = N_{||}\sum_{\mathbf{g}}\delta(\mathbf{k}_{2||}-\mathbf{k}_{1||}-\mathbf{g}), \quad (69)$$

where $\mathbf{g}$ is a vector in the two-dimensional reciprocal lattice of the subplane, and note that in passing to the

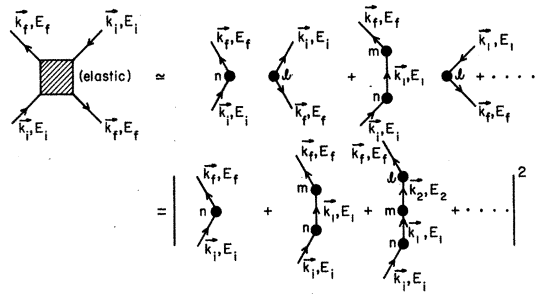

FIG. 5. Approximate diagrammatic equation for the elastic scattering cross section. Diagrams containing internal phonon lines have been neglected on the grounds that they are small.

continuum limit

$$\sum_{\mathbf{k}} \rightarrow \int (dk)/(2\pi)^3, \tag{70a}$$

$N_{||}$ becomes

$$N_{||} \rightarrow (2\pi)^2/A, \tag{70b}$$

where A is the area of a primitive unit cell of the subplane.

We obtain from Eq. (68)

$$R(\mathbf{k}_f, \mathbf{k}_i; E_i) = N_{||} \sum_{\lambda} \sum_{\mathbf{g}} \exp[-i(k_{f\perp} - k_{i\perp}) d_\lambda - i\mathbf{g}\cdot\mathbf{a}\lambda] \times T_\lambda(\mathbf{k}_f, \mathbf{k}_i; E_i)\delta(\mathbf{k}_{f||} - \mathbf{k}_{i||} - \mathbf{g}), \tag{71}$$

where

$$T_\lambda(\mathbf{k}_f, \mathbf{k}_i; E_1) = \tau_\lambda(\mathbf{k}_f, \mathbf{k}_i; E_i) + \sum_{\mathbf{k}} \sum_{\lambda_1;\ \lambda_1 \neq \lambda} \tau_\lambda(\mathbf{k}_f, \mathbf{k}; E_i) \times G^{\lambda\lambda_1}(\mathbf{k}, \mathbf{k}_i; E_i) T_\lambda(\mathbf{k}, \mathbf{k}_i; E_i), \tag{72}$$

$$\tau_\lambda(\mathbf{k}_f, \mathbf{k}_i; E_i) = b_\lambda(\mathbf{k}_f, \mathbf{k}_i; E_i) + \sum_{\mathbf{k}} b_\lambda(\mathbf{k}_f, \mathbf{k}; E_i) \times G^{\mathrm{sp}}(\mathbf{k}, \mathbf{k}_i; E_i)\tau_\lambda(\mathbf{k}, \mathbf{k}_i; E_i), \tag{73}$$

$$G^{\lambda\lambda_1}(\mathbf{k}, \mathbf{k}_i; E_i) = \sum_{\mathbf{P}} \exp\{-i(\mathbf{k}_{||} - \mathbf{k}_{i||})\cdot[\mathbf{P} + \mathbf{a}(\lambda_1 - \lambda)] - i(k_\perp - k_{i\perp})(d_{\lambda_1} - d_\lambda)\} G(\mathbf{k}, E_i), \tag{74}$$

and

$$G^{\mathrm{sp}}(\mathbf{k}, \mathbf{k}_i; E_i) = \sum_{\mathbf{P}\neq 0} \exp[-i(\mathbf{k}_{||} - \mathbf{k}_{i||})\cdot\mathbf{P}] G(\mathbf{k}; E_i). \tag{75}$$

In Eqs. (74) and (75), $\mathbf{P}$ is a vector in the Bravais net of the individual (identical) subplanes.

Equations (62) and (71)–(75) completely define the elastic scattering cross section—including its temperature dependence. As noted earlier, they are similar in structure to the set of equations first written down by Beeby[7] for a muffin-tin potential. In a subsequent paper[29] we present a solution of these equations. However, in our present context they constitute the final formal results on which our detailed analysis of the effects of lattice vibrations on LEED is based.

VII. SUMMARY

In this paper we have developed a general diagrammatic perturbation theory for the differential scattering cross section in which the effects of multiple scattering and lattice vibrations are included simultaneously. The formalism is set up to allow for the inclusion of surface as well as bulk phonon modes. It was found that the rigid-lattice ion-core potential is renormalized by a factor characterizing the mean-square vibrational amplitude of the site. The various renormalizations characteristic of the theory were discussed and an approximate set of integral equations relating the elastic scattering cross section to the ion-core potentials was derived. The relation of our general theory to earlier Born-approximation analysis[11–17] of phonon effects in LEED was displayed in detail. The consequences of the interaction of the incident electron with the conduction electrons in the solid were not examined because they are not required for the specification of the formal results given here. In the subsequent papers in this series the electron-electron interactions will be described using the inelastic collision model as proposed by Duke and co-workers.[8,9]

Finally, although we have not been concerned specifically with the energy-band structure of the solid, it is obvious that our temperature-dependent effective potential

$$v(\mathbf{k}, T) = \exp[-W(\mathbf{k}, T)] v_{\mathrm{k}} \tag{76}$$

also has consequences for such calculations. In particular, Eq. (76) predicts a temperature dependence for the energy-band gaps in solids in addition to that usually calculated by second-order perturbation theory in the electron-phonon interaction.[30] The consequences of Eq. (76) on the energy-band gaps in PbTe have been investigated by Keffer *et al.*,[31] who proposed it on the basis of an unpublished analysis of Yu.[32] They found the temperature dependence of the band gaps near L in PbTe were adequately described by Eq. (76) although its use to describe other materials is not customary.[30,33]

ACKNOWLEDGMENT

We are indebted to Dr. Wolfgang Götze for pointing out the correlation function approach which led to the work in Appendix A.

APPENDIX A

In this section we consider the evaluation of the thermal average of the exponentials containing the lattice displacement operators.

For notational simplicity we shall write the ion displacement operator at time t_1 and corresponding to the site at equilibrium position $\mathbf{R}_1^0$ as

$$\mathbf{u}(1) \equiv \mathbf{u}(\mathbf{R}_1^0, t_1). \tag{A1}$$

We wish to consider the general function

$$\mathfrak{F}_n(1, 2, \ldots, n) \equiv \langle \exp[i\mathbf{q}_1\cdot\mathbf{u}(1)] \times \exp[i\mathbf{q}_2\cdot\mathbf{u}(2)]\cdots\exp[i\mathbf{q}_n\cdot\mathbf{u}(n)]\rangle_T, \tag{A2}$$

where $\langle\cdots\rangle_T$ indicates an average over a thermal ensemble using a harmonic Hamiltonian such as given in Eq. (1). We also define the phonon propagator as

$$D^{\alpha\beta}(1, 2) = -i\langle u^\alpha(1) u^\beta(2)\rangle_T. \tag{A3}$$

We first consider $\mathfrak{F}_1(1)$.

$$\mathfrak{F}_1(1) = \langle \exp[i\mathbf{q}_1\cdot\mathbf{u}(1)]\rangle_T = \sum_{n=0}^{\infty} (n!)^{-1} \langle (iq_1{}^\alpha u(n^\alpha)^n\rangle_T, \tag{A4}$$

where the last expression follows from expanding the exponential. Using the harmonic Hamiltonian, the thermal average of a product of an odd number of

displacement operators is zero. Hence,

$$\mathfrak{F}_1(1)=\sum_{n=0}^{\infty}\frac{(-1)^n}{(2n)!}\langle(q_1{}^{\alpha}u^{\alpha}(1))^{2n}\rangle. \tag{A5}$$

We next make use of the fact that in the harmonic approximation, a thermal average of $2n$ displacement operators can be written as the sum of all possible permutations of the thermal averages of pairs of the operators.[34] The basic ordering of the operators in a given two-point correlation function is the same as it occurred in the $2n$-point correlation functions; i.e.,

$$\begin{aligned}\langle u^{\alpha}(1)u^{\beta}(2)u^{\gamma}(3)u^{\delta}(4)\rangle_T&=\langle u^{\alpha}(1)u^{\beta}(2)\rangle_T\langle u^{\gamma}(3)u^{\delta}(4)\rangle_T\\&+\langle u^{\alpha}(1)u^{\gamma}(3)\rangle_T\langle u^{\beta}(2)u^{\delta}(4)\rangle_T\\&+\langle u^{\alpha}(1)u^{\delta}(4)\rangle_T\langle u^{\beta}(2)u^{\gamma}(3)\rangle_T.\end{aligned} \tag{A6}$$

In Eq. (A5) the operators are identical, so there are $(2n)!/n!2^n$ ways of factorizing the $\langle(q_1{}^{\alpha}u^{\alpha}(1))^{2n}\rangle_T$ into a product of n two-point correlation functions $\langle(q_1{}^{\alpha}u^{\alpha}(1))^2\rangle_T$. [There are $(2n)!$ ways of permuting the operators but this overcounts since there are $n!$ ways of ordering the $\langle(q_1{}^{\alpha}u^{\alpha}(1))^2\rangle_T$ terms and two ways of ordering the $u^{\alpha}(1)$'s in a given $\langle(q_1{}^{\alpha}u^{\alpha}(1))^2\rangle_T$ term.] Therefore Eq. (A5) becomes

$$\begin{aligned}\mathfrak{F}_1(1)&=\sum_{n=0}^{\infty}\frac{(-1)^n}{(2n)!}\left[\frac{(2n!)}{n!2^n}\right]\langle(q_1{}^{\alpha}u^{\alpha}(1))^2\rangle_T{}^n\\&=\sum_{n=0}^{\infty}\frac{(-1)^n}{n!}\langle\tfrac{1}{2}(q_1{}^{\alpha}u^{\alpha}(1))^2\rangle_T{}^n\\&=\exp[-\tfrac{1}{2}\langle(q_1{}^{\alpha}u^{\alpha}(1))^2\rangle_T]\equiv\exp[-W_1(\mathbf{q}_1)].\end{aligned} \tag{A7}$$

At the end of this section we show that $W_1(\mathbf{q}_1)$ becomes the familiar Debye-Waller factor when the Debye model of the phonon spectrum is assumed.

We next consider

$$\mathfrak{F}_2(1,2)-\langle\exp[iq_1{}^{\alpha}u^{\alpha}(1)]\exp[iq_2{}^{\beta}u^{\beta}(2)]\rangle_T. \tag{A8}$$

Expanding the exponetials in Eq. (A8), we obtain

$$\mathfrak{F}_2(1,2)=\sum_{n=0}^{\infty}\sum_{m=0}^{\infty}(n!)^{-1}(m!)^{-1}\times\langle(iq_1{}^{\alpha}u^{\alpha}(1))^n(iq_2{}^{\beta}u^{\beta}(2))^m\rangle_T. \tag{A9}$$

The contribution of a given term in the series is zero unless $(n+m)$ is an even number. Each nonzero term can be factorized into a product of two-point correlation functions such as exhibited in Eq. (A6). We classify terms in the expansion of Eq. (A9) according to the number of linked two-point correlation functions that they contain. A linked two-point correlation function is one which contains a term from $\mathbf{u}(1)$ and a term from $\mathbf{u}(2)$; i.e.,

$$(i)^2q_1{}^{\alpha}\langle u^{\alpha}(1)u^{\beta}(2)\rangle_Tq_2{}^{\beta}\equiv(-i)q_1{}^{\alpha}D^{\alpha\beta}(1,2)q_2{}^{\beta} \tag{A10}$$

is such a linked function.

We define $F_2{}^{(j)}(1,2)$ as the sum of all terms in Eq. (A9) that contain "j" linked two-point correlation functions. Consider first the terms involving no linked correlation functions,

$$F_2{}^{(0)}(1,2)=[\sum_{n=0}^{\infty}\sum_{m=0}^{\infty}(n!)^{-1}(m!)^{-1}\times\langle(iq_1{}^{\alpha}u^{\alpha}(1))^n(iq_2{}^{\beta}u^{\beta}(2))^m\rangle]|_{\text{nfl}}, \tag{A11}$$

where nfl denotes no linked functions. Only those terms for which "n" and "m" both are even contribute to Eq. (A11). Hence, we can write

$$\begin{aligned}F_2{}^{(0)}(1,2)&=\{\sum_{n=0}^{\infty}[(2n)!]^{-1}\langle(iq_1{}^{\alpha}u^{\alpha}(1))^{2n}\rangle_T\}\\&\times\{\sum_{n=0}^{\infty}[(2m)!]^{-1}\langle(iq_2{}^{\beta}u^{\beta}(2))^{2m}\rangle_T\}\\&=\mathfrak{F}_1(1)\mathfrak{F}_1(2)\\&=\exp[-W_1(\mathbf{q}_1)]\exp[-W_2(\mathbf{q}_2)].\end{aligned} \tag{A12}$$

Consider next the terms involving a single linked correlation function. When forming the linked function from the terms in Eq. (A9), we can choose the $u^{\alpha}(1)$ term in "n" ways and the $u^{\beta}(2)$ term in "m" ways. We obtain

$$\begin{aligned}F_2{}^{(1)}(1,2)&=\sum_{n=1}^{\infty}\sum_{m=1}^{\infty}(n!)^{-1}(m!)^{-1}(i)^2\\&\times\langle q_1{}^{\alpha}u^{\alpha}(1)u^{\beta}(2)q_2{}^{\beta}\rangle_T(mn)\\&\times[\langle(iq_1{}^{\alpha}u^{\alpha}(1))^{n-1}(iq_2{}^{\beta}u^{\beta}(2))^{m-1}\rangle_T]|_{\text{nfl}}\\&=(-i)q_1{}^{\alpha}D^{\alpha\beta}(1,2)q_2{}^{\beta}\\&\times\{\sum_{n=1}^{\infty}\sum_{m=1}^{\infty}[(n-1)!]^{-1}[(m-1)!]^{-1}\\&\times\langle(iq_1{}^{\alpha}u^{\alpha}(1))^{n-1}(iq_2{}^{\beta}u^{\beta}(2))^{m-1}\rangle_T\}|_{\text{nfl}}\end{aligned} \tag{A13}$$

Note the change on the lower limit of the sums since we must have at least $m=1$, $n=1$ to get a linked function. We next change variables

$$n'=n-1, \tag{A14}$$

$$m'=m-1 \tag{A15}$$

to obtain

$$\begin{aligned}F^{(1)}(1,2)&=-iq_1{}^{\alpha}D^{\alpha\beta}(1,2)q_2{}^{\beta}\{\sum_{n'=0}^{\infty}\sum_{m'=0}^{\infty}(n'!)^{-1}(m'!)^{-1}\\&\langle(iq_1{}^{\alpha}u^{\alpha}(1))^{n'}(iq_2{}^{\beta}u^{\beta}(2))^{m'}\rangle_T\}|_{\text{nfl}}\\&=-iq_1{}^{\alpha}D^{\alpha\beta}(1,2)q_2{}^{\beta}F_2{}^{(0)}(1,2).\end{aligned} \tag{A16}$$

$F_2{}^{(2)}(1,2)$ is the sum of terms in Eq. (A9) involving two linked correlation functions. From a given term in Eq. (A9) we can form the two linked correlation functions in $n(n-1)m(m-1)/2!$ ways. (The factor of $1/2!$ comes in since the order of the two linked correlation

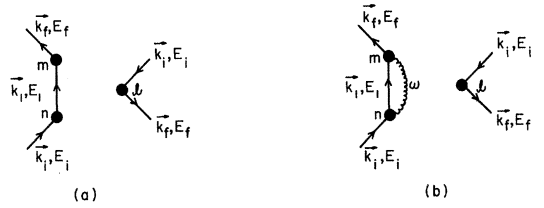

FIG. 6. Diagrams contributing to the electric scattering cross section that illustrate the effect of adding a phonon propagator to a "bare" diagram. (a) is the "bare" diagram which is evaluated in Eq. (B1) and (b) is that evaluated in Eq. (B2).

functions does not matter.) We thus obtain

$$F_2^{(2)}(1,2)=\sum_{n=2}^{\infty}\sum_{m=2}^{\infty}(n')^{-1}(m')^{-1}\left(\frac{n(n-1)m(m-1)}{2!}\right)\times[(i)^2\langle q_1{}^\alpha u^\alpha(1)u^\beta(2)q_2{}^\beta\rangle_T{}^2]\times[\langle(iq_1{}^\alpha u^\alpha(1))^{n-2}(iq_2{}^\beta u^\beta(2))^{m-2}\rangle_T]|_{\mathrm{nfl}}=\frac{[-iq_1{}^\alpha D^{\alpha\beta}(1,2)q_2{}^\beta]^2}{2!}F_2^{(0)}(1,2). \quad \text{(A17)}$$

In a completely analogous manner we obtain for the sum of terms involving "j" linked functions

$$F_2^{(j)}(1,2)=\{[-iq_1{}^\alpha D^{\alpha\beta}(1,2)q_2{}^\beta]^j/j!\}F_2^{(0)}(1,2). \quad \text{(A18)}$$

We now explicitly sum the $F_2^{(j)}(1,2)$ to obtain $\mathfrak{F}_2(1,2)$:

$$\mathfrak{F}_2(1,2)=\sum_{j=0}^{\infty}F_2^{(j)}(1,2)=F_2^{(0)}(1,2)\sum_{j=0}^{\infty}\frac{[-iq_1{}^\alpha D^{\alpha\beta}(1,2)q_2{}^\beta]^j}{j!}=F_2^{(0)}(1,2)\exp[-iq_1{}^\alpha D^{\alpha\beta}(1,2)q_2{}^\beta]=\exp[-W_1(\mathbf{q}_1)]\exp[-W_2(\mathbf{q}_2)]\times\exp[-iq_1{}^\alpha D^{\alpha\beta}(1,2)q_2{}^\beta]. \quad \text{(A19)}$$

The general case of N exponentials is equally straightforward. We define

$$\mathfrak{F}_N(1,2,\ldots,N)=\langle\exp[i\mathbf{q}_1\cdot\mathbf{u}(1)]\exp[i\mathbf{q}_2\cdot u(2)]\cdots\exp[i\mathbf{q}_N\cdot\mathbf{u}(N)\rangle_T=\sum_{n_1=0}^{\infty}\sum_{n_2=0}^{\infty}\cdots\sum_{n_N=0}^{\infty}[(n_1!)^{-1}(n_2!)^{-1}\cdots(n_N!)^{-1}]\times\langle(iq_1{}^\alpha u^\alpha(1))^{n_1}(iq_2{}^\beta u^\beta(2))^{n_2}\cdots(iq_N{}^\gamma u^\gamma(N))^{n_N}\rangle_T. \quad \text{(A20)}$$

Again, we classify terms as to the number and kind of linked two-point correlation functions that they contain when they are expanded in terms of products of these functions. We define the sum of the terms having $j_{1,2}$ linked functions involving $\mathbf{u}(1)$ and $\mathbf{u}(2)$, $j_{1,3}$ linked functions involving $\mathbf{u}(1)$ and $\mathbf{u}(3)$, ..., and $j_{N-1,N}$ linked functions involving $\mathbf{u}(N-1)$ and $\mathbf{u}(N)$ as

$$F_N^{(j_{1,2},j_{1,3},\cdots j_{N-1,N})}(1,2,\ldots,N).$$

By an extension of the argument leading to Eqs. (A7) and (A11) we find

$$F_N^{(0,0,\cdots,0)}(1,2,\ldots,N)=\mathfrak{F}_1(1)\mathfrak{F}_1(2)\cdots\mathfrak{F}_1(N)=\exp[-W_1(\mathbf{q}_1)]\exp[-W_2(\mathbf{q}_2)]\cdots\exp[-W_N(\mathbf{q}_N)]. \quad \text{(A21)}$$

The same procedure as used above gives for a general term

$$F_N^{(j_{1,2},j_{1,3},\ldots j_{N-1,N})}(1,2,\ldots,N)=\frac{[-iq_1{}^\alpha D^{\alpha\beta}(1,2)q_2{}^\beta]^{j_{1,2}}}{j_{1,2}!}\times\frac{[iq_1{}^\alpha D^{\alpha\beta}(1,3)q_3{}^\beta]^{j_{1,3}}}{j_{1,3}!}\cdots\frac{[-iq_{N-1}{}^\alpha D^{\alpha\beta}(N-1,N)q_N{}^\beta]^{j_{N-1,N}}}{j_{N-1,N}!}\times F_N^{(0,0,\ldots,0)}(1,2,\ldots,N). \quad \text{(A22)}$$

From Eq. (A22) we obtain

$$\mathfrak{F}_N(1,2,\ldots,N)=\sum_{j_{1,2}=0}^{\infty}\sum_{j_{1,3}=0}^{\infty}\cdots\sum_{j_{N-1,N}=0}^{\infty}F_N^{(j_{1,2},j_{1,3},\ldots,j_{N-1,N})}(1,2,\ldots,N)=F_N^{(0,0,\ldots,0)}(1,2,\ldots,N)\exp[-iq_1{}^\alpha D^{\alpha\beta}(1,2)q_2{}^\beta]\times\exp[iq_1{}^\alpha D^{\alpha\beta}(1,3)q_3{}^\beta]\cdots\exp[-iq_{N-1}{}^\alpha D^{\alpha\beta}(N-1,N)q_N{}^\beta]. \quad \text{(A23)}$$

This argument completes the derivation of Eq. (21), and of the general diagrammatic expansion of Sec. III.

We conclude this Appendix by evaluating $W_1(\mathbf{q}_1)$ using the Debye model of the phonon spectrum. From Eqs. (22) and (A7)

$$W_1(\mathbf{q}_1)=\tfrac{1}{2}q_1{}^\alpha\langle u_1{}^\alpha u_1{}^\beta\rangle_T q_1{}^\beta=\tfrac{1}{2}iq_1{}^\alpha D^{\alpha\beta}(1,1)q_1{}^\beta. \quad \text{(A24)}$$

In the Debye model we assume an isotropic phonon spectrum. In this case we obtain[26]

$$D^{\alpha\beta}(1,2)=N\sum_{\mathbf{k}}\int(d\omega/2\pi)\times\exp[i\mathbf{k}\cdot(\mathbf{R}_1{}^0-\mathbf{R}_2{}^0)-i\omega(t_1-t_2)]D^{\alpha\beta}(\mathbf{k},\omega), \quad \text{(A25)}$$

where

$$D^{\alpha\beta}(\mathbf{k},\omega)=[i\hbar\delta_{\alpha,\beta}(2\pi)/2M\omega(\mathbf{k})][N(-\omega)]\times[\delta(\omega-\omega(\mathbf{k}))-\delta(\omega+\omega(\mathbf{k}))], \quad \text{(A26)}$$

$$N(\omega)=[\exp(\hbar\omega/k_BT)-1]^{-1}, \quad \text{(A27)}$$

where M is the ion mass, $\omega(\mathbf{k})$ is the frequency spectrum, and $\delta_{\alpha,\beta}$ is the Kronecker δ. Substituting Eqs. (A25) and (A26) into Eq. (A24), we obtain

$$W_1(\mathbf{q}_1)|_{\mathrm{Debye}}=(\hbar q_1{}^2/4MN)\sum_{\mathbf{k}}[\omega(\mathbf{k})]^{-1}\times\{N[-\omega(\mathbf{k})]-N[\omega(\mathbf{k})]\}=(\hbar q_1{}^2/4MN)\sum_{\mathbf{k}}[\omega(\mathbf{k})]^{-1}\times\{2N[\omega(k)]+1\}. \quad \text{(A28)}$$

Passing to the continuum limit in Eq. (A27), we take

$$\sum_{\mathbf{k}} \rightarrow V \int_0^{k_D} \frac{dk\, k^2}{(2\pi)^3} \int d\Omega \sum_{\lambda_{\mathbf{k}}},$$

where V is the volume of the system, $\lambda_{\mathbf{k}}$ is the phonon polarization index, and k_D is the cutoff wave vector defined by

$$\sum_{\mathbf{k}} = N = k_D^3/2\pi^2. \tag{A29}$$

The phonon dispersion relation in the Debye approximation is given by

$$\omega(\mathbf{k}) = v_s k, \tag{A30}$$

where v_s is an average sound velocity. We thus obtain from Eq. (A27)

$$W_1(\mathbf{q}_1)|_{\text{Debye}} = \frac{3\hbar q_1^2 V}{MNv_s 4\pi^2} \times \int_0^{k_D} dk\, k \left[\frac{1}{\exp(v_s k/k_B T)-1} + \frac{1}{2}\right], \tag{A31}$$

and in terms of the Debye temperature defined by

$$\Theta_D = \hbar v_s q_D/k_B, \tag{A32}$$

Eq. (A31) may be rewritten as

$$W_1(\mathbf{q}_1) = \frac{3\hbar^2 q_1^2}{2Mk_B\Theta_D}\left[\frac{1}{4} + \left(\frac{T}{\Theta_D}\right)^2 \int_0^{\Theta_D/T} dx \frac{x}{e^x-1}\right], \tag{A33}$$

which is the expression for the Debye-Waller factor. Strictly speaking, $\exp[-2W(\mathbf{q}_1)]$ is referred to as the Debye-Waller factor[35] in the literature.

APPENDIX B

In this Appendix we show that the contribution of a diagram containing explicit phonon propagators to the elastic scattering cross section usually is small compared to the corresponding "bare" diagram. In particular we consider the diagrams in Fig. 6 in order to provide an order-of-magnitude estimate of the size of this phenomenon.

The contribution of the "bare" diagram in Fig. 6(a) is

$$R_a = [m^2/(2\pi\hbar^2)^2]\delta(E_i-E_f) \sum_{l,m,n;\ m\neq n} \sum_{\mathbf{k}_1} B(n;\mathbf{k}_i,\mathbf{k}_1;E_i) \times G(\mathbf{k}_1,E_i) B(m;\mathbf{k}_1,\mathbf{k}_f;E_i) B^*(l;\mathbf{k}_i,\mathbf{k}_f;E_i), \tag{B1}$$

whereas the contribution of the diagram in Fig. 6(b) is

$$R_b = [m^2/(2\pi\hbar^2)^2]\delta(E_i-E_f) \times \sum_{l,m,n;\ m\neq n} \sum_{\mathbf{k}_1} \int \frac{d\omega}{2\pi} B(n;\mathbf{k}_i,\mathbf{k}_1;E_i) G(\mathbf{k}_1,E_i-\hbar\omega) \times B(m;\mathbf{k}_1,\mathbf{k}_f;E_i-\hbar\omega) B^*(l;\mathbf{k}_i,\mathbf{k}_f;E_i) \times (-i\hbar)(k_f-k_1)^\alpha D^{\alpha\beta}(m,n;\omega)(k_1-k_i)^\beta. \tag{B2}$$

A typical phonon energy is on the order of $k_B\Theta_D$ so $E_i \gg \hbar\omega$ for any experimental situation. Hence, in Eq. (B2) we may take

$$E_i - \hbar\omega \cong E_i. \tag{B3}$$

This approximation leads to the result

$$R_b \cong R_a\left[(-i\hbar)\int \frac{d\omega}{2\pi} Q^\alpha D^{\alpha\beta}(m,n;\omega) Q^\beta\right] \equiv R_a C, \tag{B4}$$

where Q is a typical momentum transfer at a scattering vertex. As we are interested only in an order-of-magnitude estimate of the coefficient C in Eq. (B4), we shall use the Debye model of the solid in our evaluation of C. The relevant quantities are defined in Eqs. (A25) and (A26). We obtain the expression for the coefficient

$$C \equiv (-i)\int \frac{d\omega}{2\pi} Q^\alpha D^{\alpha\beta}(m,n;\omega) Q^\beta = -\frac{\hbar Q^2}{2MN} \sum_{\mathbf{k}} \frac{\exp[i\mathbf{k}\cdot(\mathbf{R}_m^0-\mathbf{R}_n^0)]}{\omega(\mathbf{k})} \times \left(\frac{2}{\exp[\hbar\omega(\mathbf{k})/k_B T]-1}+1\right). \tag{B5}$$

Passing to the continuum limit as in Eq. (A28) and taking

$$\omega(\mathbf{k}) = v_s k, \tag{B6}$$

we obtain

$$C = -\frac{3\hbar Q^2 V}{MNv_s}\int_0^{k_D} \frac{dk\, k}{(2\pi)^3} \times \left(\frac{1}{\exp[\hbar v_s k/k_B T]-1}+\frac{1}{2}\right)\frac{\sin[k\,|\,\mathbf{R}_m^0-\mathbf{R}_n^0\,|]}{k\,|\,\mathbf{R}_m^0-\mathbf{R}_n^0\,|}. \tag{B7}$$

In Eq. (B7) we perform the integral involving the constant term to obtain

$$\int_0^{k_D} \frac{dk}{4\pi^2} \frac{\sin[k\,|\,\mathbf{R}_m^0-\mathbf{R}_n^0\,|]}{|\,\mathbf{R}_m^0-\mathbf{R}_n^0\,|} = \frac{\{1-\cos[k_D\,|\,\mathbf{R}_m^0-\mathbf{R}_n^0\,|]\}}{4\pi^2\,|\,\mathbf{R}_m^0-\mathbf{R}_n^0\,|^2}. \tag{B8}$$

Next, we note that in the high-temperature limit,

$$\frac{1}{\exp(\hbar v_s k/k_B T)-1} \leq \frac{k_B T}{\hbar v_s k} \tag{B9}$$

and so most of the contribution to the other integral in

Eq. (B7) will come from k near zero. Hence, let us approximate

$$\int_0^{k_D} \frac{dk}{2\pi} \frac{\sin[k \mid \mathbf{R}_m^0 - \mathbf{R}_n^0 \mid]}{\mid \mathbf{R}_m^0 - \mathbf{R}_n^0 \mid} \frac{1}{\exp(\hbar v_s k/k_B T) - 1} \simeq \frac{k_B T}{2\pi^2 \hbar v_s \mid \mathbf{R}_m^0 - \mathbf{R}_n^0 \mid} \int_0^{k_D} \frac{\sin[k \mid \mathbf{R}_m^0 - \mathbf{R}_n^0 \mid]}{k} dk$$

$$= \frac{k_B T}{2\pi^2 \hbar v_s \mid \mathbf{R}_m^0 - R_n^0 \mid} \mathrm{Si}(k_D \mid \mathbf{R}_m^0 - \mathbf{R}_n^0 \mid), \tag{B10}$$

where the last expression in Eq. (B10) follows from the definition of the sine integral.[36] From Eqs. (B8) and (B10) we obtain

$$\mid C \mid \simeq \frac{3\hbar Q^2 V}{2\pi^2 M N v_s \mid \mathbf{R}_m^0 - \mathbf{R}_n^0 \mid} \left[\frac{[1 - \cos(k_D \mid \mathbf{R}_m^0 - \mathbf{R}_n^0 \mid)]}{2 \mid \mathbf{R}_m^0 - \mathbf{R}_n^0 \mid} + \left(\frac{k_B T}{\hbar v_s} \right) \mathrm{Si}(k_D \mid \mathbf{R}_m^0 - \mathbf{R}_n^0 \mid) \right]$$

$$= \frac{3\hbar^2 Q^2}{M k_B \Theta_D k_D^2 \mid \mathbf{R}_m^0 - \mathbf{R}_n^0 \mid} \left(\frac{[1 - \cos(k_D \mid \mathbf{R}_m^0 - \mathbf{R}_n^0 \mid)]}{2 \mid \mathbf{R}_m^0 - \mathbf{R}_n^0 \mid} + \frac{k_D T}{\Theta_D} \mathrm{Si}(k_D \mid \mathbf{R}_m^0 - \mathbf{R}_n^0 \mid) \right). \tag{B11}$$

Taking "typical" values of

$\hbar^2 Q^2/2m \simeq 25$ eV, $\Theta_D \simeq 300$°K, $T \simeq 300$°K,

$\mid \mathbf{R}_m^0 - \mathbf{R}_n^0 \mid \simeq 4$ Å, $M \simeq 100$ amu, $k_D \simeq 1$ Å^{-1},

we obtain

$$\mid C \mid \simeq 10^{-2}, \tag{B12}$$

which means

$$R_a \gg R_b \tag{B13}$$

and so it is reasonable to neglect the diagram in Fig. 6(b) when compared with the diagram in Fig. 6(a). Diagrams containing "n" phonon lines will have a contribution roughly equal to the "bare" diagram contribution multiplied by $\mid C \mid^n$ and so become completely negligible as "n" becomes large. Hence, in evaluating the elastic scattering cross section, it is reasonable to consider only the "bare" diagrams shown in Fig. 5. It is important to observe, however, that the magnitude of C depends on $\hbar^2 Q^2/2M$. Thus for large momentum transfers (as encountered, e.g., Bragg scattering at high energies), the contributions from diagrams containing internal phonon propagators can become large. In this case, one should view the approximation for the elastic scattering vertex developed in Sec. V with caution.

* This research was supported in part by the Advanced Research Projects Agency under Contract No. SD-131.

† NSF Postdoctoral Fellow.

[1] E. G. McRae, J. Chem. Phys. **45,** 3258 (1966); Surface Sci. **8,** 14 (1967).
[2] K. Hirabayashi and Y. Takeishi, Surface Sci. **4,** 150 (1966).
[3] D. S. Boudreaux and V. Heine, Surface Sci. **8,** 426 (1967).
[4] F. Hofmann and H. P. Smith, Jr., Phys. Rev. Letters **19,** 1479 (1967).
[5] P. M. Marcus and D. W. Jepsen, Phys. Rev. Letters **20,** 925 (1967).
[6] J. S. Plaskett, Proc. Roy. Soc. (London) **A301,** 363 (1967).
[7] J. L. Beeby, J. Phys. C **1,** 82 (1968).
[8] C. B. Duke and C. W. Tucker, Jr., Surface Sci. **15,** 231 (1969); Phys. Rev. Letters **23,** 1163 (1969).
[9] C. B. Duke, J. R. Anderson, and C. W. Tucker, Jr., Surface Sci. **19,** 117 (1970).
[10] A. U. MacRae, Surface Sci. **2,** 522 (1964).
[11] E. R. Jones, J. T. McKinney, and M. B. Webb, Phys. Rev. **151,** 476 (1966).
[12] J. T. McKinney, E. R. Jones, and M. B. Webb, Phys. Rev. **160,** 523 (1967).
[13] R. M. Goodman, H. H. Farrell, and G. A. Somorjai, J. Chem. Phys. **48,** 1046 (1968).
[14] R. F. Barnes, M. G. Lagally, and M. B. Webb, Phys. Rev. **171,** 627 (1968).
[15] J. M. Morabito, Jr., R. F. Steiger, and G. A. Somorjai, Phys. Rev. **179,** 638 (1969).
[16] H. Yoshioka and Y. Kainuma, J. Phys. Soc. Japan **17,** 134 (1962).
[17] R. F. Wallis and A. A. Maradudin, Phys. Rev. **148,** 962 (1966).
[18] See, for example, I. H. Khan, J. P. Hobson, and R. A. Armstrong, Phys. Rev. **129,** 1513 (1963); G. Gafner, Surface Sci. **19,** 9 (1970).
[19] See, for example, S. S. Schweber, *An Introduction to Relativistic Quantum Field Theory* (Row, Peterson, and Co., Evanston, Ill., 1961), Chap. 11.
[20] B. C. Clark, R. Herman, and R. F. Wallis, Phys. Rev. **139,** A860 (1965).
[21] R. F. Wallis and A. A. Maradudin, Phys. Rev. **148,** 962 (1966).
[22] R. F. Wallis, B. C. Clark, R. Herman, and D. C. Gazis, Phys. Rev. **180,** 716 (1969).
[23] D. Pines, *The Many-Body Problem* (Benjamin, New York, 1962).
[24] W. A. Harrison, *Pseudopotentials in the Theory of Metals* (Benjamin, New York, 1966).
[25] A. A. Abrikosov, L. P. Gor'kov, and I. Ye. Dzyaloshinskii, *Quantum Field Theoretical Methods in Statistical Physics* (Pergamon, New York, 1965).
[26] A. A. Maradudin, E. W. Montroll, and G. H. Weiss, in *Solid State Physics,* edited by F. Seitz and D. Turnbull (Academic, New York, 1963), Suppl. 3.
[27] L. I. Schiff, *Quantum Mechanics* (McGraw-Hill, New York, 1955), Chap. VIII.
[28] See, for example, C. Kittel, *Introduction to Solid State Physics* (Wiley, New York, 1963), Chap. 6.
[29] G. E. Laramore and C. B. Duke, Phys. Rev. B (to be published).
[30] G. D. Mahan, J. Phys. Chem. Solids **26,** 751 (1965).
[31] C. Keffer, T. M. Hayes, and A. Bienenstock, Phys. Rev. Letters **21,** 1676 (1968).
[32] S. C. Yu (unpublished).
[33] Y. P. Varshni, Physica **34,** 149 (1967).
[34] This is merely a consequence of Wick's theorem. See, for example, Ref. 25, Chap. 2.
[35] C. Kittel, *Quantum Theory of Solids* (Wiley, New York, 1963), Chaps. 19–20.
[36] E. Jahnke and F. Emde, *Tables of Functions* (Dover, New York, 1945), Chap. I.